Standing Wave Design of Nonlinear SMB Systems for Fructose Purification

T. Mallmann and B. D. Burris
U. S. Filter, 4669 Shepherd Trail, Rockford, IL 61105

Z. Ma and N. H. L. Wang
School of Chemical Engineering, Purdue University, West Lafayette, IN 47907

Design equations were derived from standing wave analysis for continuous moving bed (CMB) and simulated moving bed (SMB) systems with nonlinear isotherms. Simple wave solutions and hodograph plots from batch elution experiments can be used to derive the optimal operation conditions for SMB systems without mass-transfer effects. The design equations are tested with results from computer simulations and experimental data from two pilot-scale SMB units for the separation of fructose from glucose. Batch equilibrium tests of single component and binary solutions are used to estimate adsorption isotherm parameters. Overall mass-transfer and axial dispersion coefficients are estimated from eight sets of pulse, frontal and elution data at different concentrations and flow rates. The isotherm and mass-transfer parameters are used in the standing wave analysis to determine the zone flow rates and switching times for the two SMB units. Experimental column profiles, product purities, and product concentrations agree closely with simulation results. This method gives robust operation conditions for SMB systems with nonlinear isotherms, and optimal cycle time and zone flow rates for nonlinear systems without mass-transfer effects can be determined from the standing wave analysis.

Introduction

Simulated moving bed (SMB) chromatography has many advantages over the conventional batch chromatography for industrial-scale separations. It is a continuous process and can separate a mixture of two similar solutes into highly pure products. It has the high yield and low solvent consumption typical of recycle chromatography (Wu et al., 1997) and the high sorbent utilization typical of a carousel process (Ernest et al., 1997). SMB also has the high product concentration and high sorbent productivity of a continuous moving bed (CMB) process without the difficulties associated with moving the solid phase in CMB. SMB can also be modified into different configurations to further improve productivity according to specific applications (Ruthven and Ching, 1989; Ganetsos and Barker, 1993). For these reasons, SMB has been used at large scale for hydrocarbon purification and sugar purification (Broughton, 1968; Broughton et al., 1970; Corbett and Burke, 1996). This study focuses on the design of nonlinear SMB systems for fructose purification.

A typical SMB system consists of a series of sorbent columns that are connected to form a circuit. The columns are divided into four zones with two input and two output ports. An example of a pilot-scale SMB for the separation of fructose from glucose is shown in Figures 1a and 1b. Such a configuration is designed to achieve binary fractionation (Ruthven and Ching, 1989; Broughton et al., 1970). The bed movement is simulated by periodically moving the inlet and outlet ports along the fluid-flow direction in the circuit. If average port movement velocity is greater than the migration velocity of the high affinity solute (E), but is less than the migration velocity of the low affinity solute (R), the solute E will lag behind and shift toward the extract port and the solute R toward the raffinate port. In order to achieve high product purity, the flow rates in the four zones have to be chosen such that the more retained solute shifts toward the extract port and stays in zone III and the less retained solute

Correspondence concerning this article should be addressed to N.-H. L. Wang.

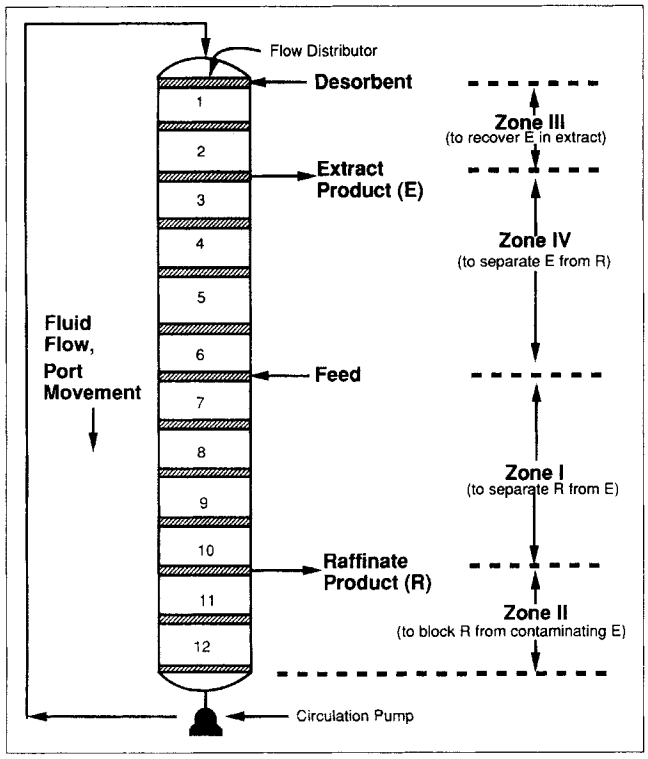

Figure 1a. Pilot-scale four-section SMB system for the separation of fructose and glucose.

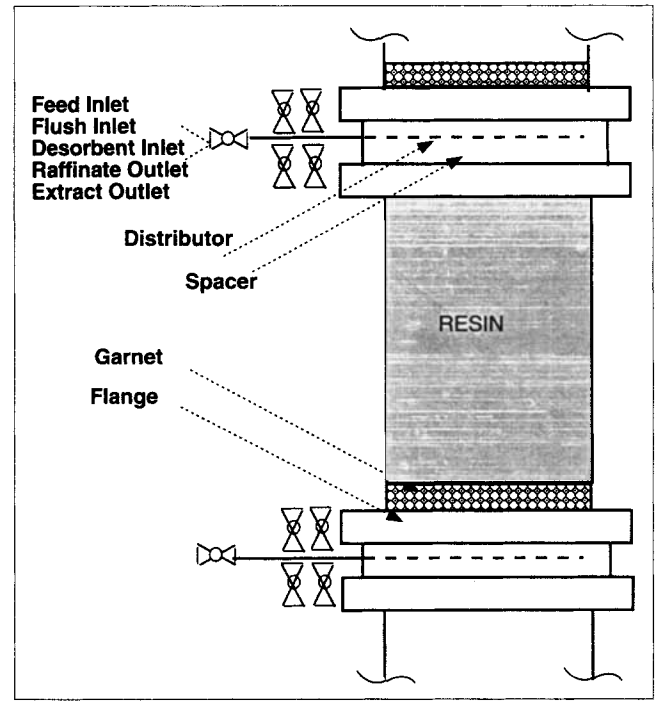

Figure 1b. One section design for the system in Figure 1a.

moves toward the raffinate port and stays in zone II (Figure 1c). The determination of an averaged port movement velocity (or port switching time) and the four zone flow rates is the key issue in SMB design.

In the literature, there are two ways to determine the flow rates and the port switching time: (1) using equilibrium theory assuming negligible mass-transfer resistances (Rhee et al., 1971; Ruthven and Ching, 1989; Storti et al., 1993, 1995); (2) using numerical solution of mathematical models to simulate the performance of SMB and to search for the flow rates and switching time that give a desired separation (Ching et al., 1988, 1989, 1991, 1993; Adachi, 1994; Ulrich and Hsu, 1989). The former can only be used in systems in which mass-transfer resistances are negligible, while the latter can be used in systems with finite-mass-transfer resistances. However, starting a simulation requires a set of flow rates and a port switching time, which are usually derived from the equilibrium analysis. In any case, equilibrium analysis is crucial for the development of robust design of nonlinear SMB systems.

In a recent study by Ma and Wang (1997), a standing wave analysis is developed for the design of CMB and SMB systems with linear isotherms either with or without mass-transfer effects. The analysis shows that by proper choices of the four flow rates and solid movement velocity in CMB (or equivalent port switching time in SMB), the advancing front (or adsorption wave) of the fast migrating solute (R) can be made standing in zone II in CMB (or standing in a time-averaged sense in SMB). The adsorption wave of the slow migrating solute (E) is made standing in zone I and its desorption wave standing in zone III (Figure 1c). For specified purities of E and R, the standing wave conditions give the maximum throughput per column volume (or column productivity), the lowest desorbent requirement, and the highest product concentrations. A set of algebraic equations have been obtained linking solute capacity factors, mass-transfer parameters (axial dispersion and lumped mass-transfer coefficients), four zone lengths, and product purities to the four zone flow rates and solid movement velocity in CMB (or port switching time in SMB). The standing wave designs were validated with literature data and computer simulations of CMB and SMB based on a linear driving force (or lumped) rate model. The analysis not only simplifies significantly the design problem involving multiple parameters for CMB and SMB systems, but also gives the optimal flow rates and switching time. In this study, the standing wave analysis is extended to nonlinear isotherm systems.

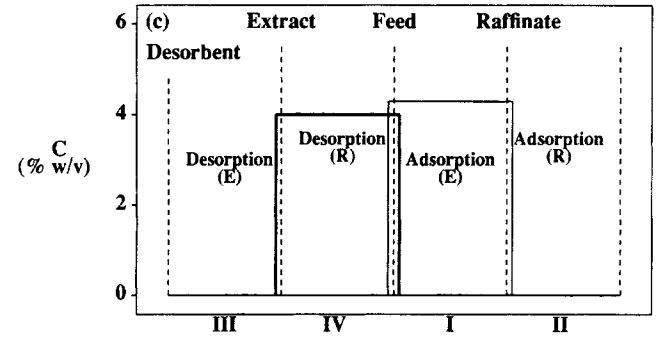

Figure 1c. Standing waves in the four zones for a linear isotherm system without mass-transfer effects.

Table 1. System and Numerical Parameters Used in Simulation for Figures 2 and 3

	Fr (ml/min)	ϵ_b	ϵ_p	ID (cm)
Column	750	0.402	0.250	16.147

Mass Transfer	E_b (cm^2/min)	K_f (l/min)	Isotherm a	Isotherm $\lvert b\rvert$*
$R = 25\ \mu$m	0.09058	45.579	0.0948	8.585×10^{-4}
$R = 50\ \mu$m	0.18040	11.650	0.3073	2.540×10^{-4}
$R = 100\ \mu$m	0.35868	2.9653		

*For simulations using anti-Langmuir isotherm the negative values are taken.

In order to achieve high throughput per column volume (or column productivity), a CMB or SMB should operate at high loadings and high feed concentrations, in which case the isotherms are often in nonlinear regions. For such systems, competition for adsorption sites significantly affects solute distribution and the migration velocities of the concentration waves. For a Langmuir isotherm system, the adsorption waves are "self sharpening," whereas the desorption waves are "proportionally broadening" (that is, wave spreading is proportional to migration distance). For example, when a large volume of a binary mixture is fed to a column and followed by washing, the elution profiles consist of six concentration waves: two shocks (one adsorption and one desorption wave) and a diffuse wave (desorption wave) for the low affinity solute; one shock (adsorption wave) and two diffuse waves (desorption waves) for the high affinity solute (Figure 2a). For a typical four zone SMB system, the migration velocities of four out of the six waves have to be identified and controlled to achieve complete separation. It is an important objective of this study to apply the standing wave analysis of nonlinear waves in CMB and SMB and develop the method for finding the optimal zone flow rates and port switching time.

In many previous studies of nonlinear countercurrent adsorption processes, a simulated moving bed process is taken as a true steady-state countercurrent process within each zone. The equilibrium theory of Rhee et al. (1971, 1989) for one-zone continuous countercurrent moving bed process is applied (Storti et al., 1989, 1993, 1995; Mazzotti et al., 1994, 1996). This study, by contrast, treats a simulated moving bed process as a dynamic chromatography process in a closed loop, except that (1) there are two inlet and two outlet ports (compared to a single inlet and a single outlet port in batch chromatography); and (2) the ports either move continuously or periodically along the fluid-flow direction. In the limit of continuous port movement, the process is equivalent to a continuous countercurrent moving bed process. If the ports move periodically, it is a simulated moving bed process. When the port movement velocity and the flow rates in the four zones in a continuous moving port process are chosen such that the four waves are standing in the appropriate zones, complete separation and high product purity are guaranteed. In an SMB, the four waves are "standing" in a time-averaged sense. This standing wave approach is simple in concept, and the calculation of zone flow rate and port movement velocity is relatively straightforward. Furthermore, the analysis can be applied to a large class of nonlinear isotherm systems, whereas the literature methods are specific to the types of isotherms

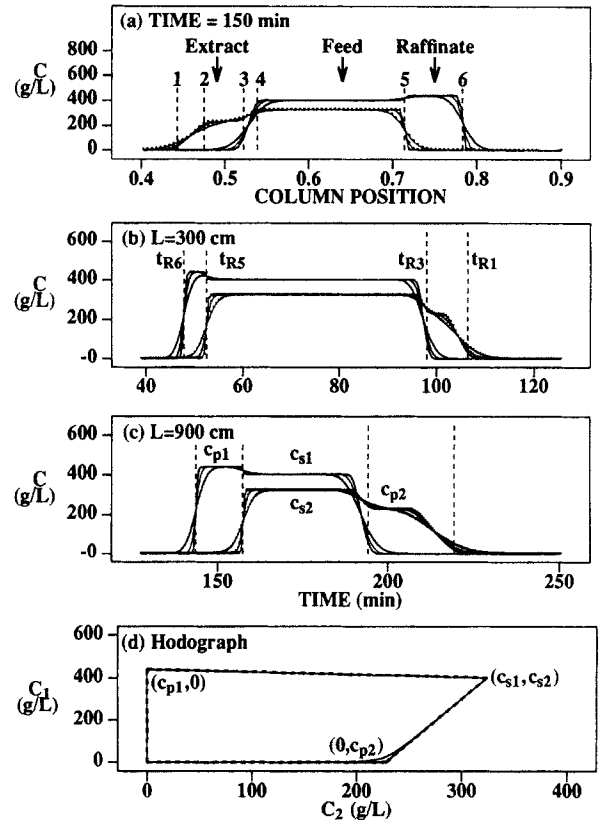

Figure 2. Concentration profiles, effluent histories, and the hodograph plot for a competitive Langmuir isotherm system of two components.

Solid lines: fast migrating solute (solute 1); dotted lines: slow migrating solute (solute 2). Three different particle sizes are used in the simulation ($d_p = 50$, 100, 200 μm). The more spread bands are obtained with the largest particles. (a) Concentration profiles in a column; (b) and (c) effluent histories of columns of different lengths; (d) hodograph plot. The simulation parameters are listed in Table 1.

considered, for example, constant separation factor isotherms (Storti et al., 1989; Mazzotti et al., 1994), Langmuir isotherms (Ching et al., 1988; Mazzotti et al., 1996), and polynomial isotherms (Ching et al., 1993).

In the following, the standing concentration wave concept is introduced for nonlinear isotherm systems without mass-transfer effects. Concentration wave velocities can be derived from batch elution data and can be used to determine the flow rates and switching time that are needed to achieve standing concentration waves. Design equations for systems with convex and concave isotherms are derived from the standing wave analysis. This analysis identifies the specific standing waves and the optimal flow rates and port switching time. The design method is subsequently tested using computer simulations based on the lumped rate model (Ma and Wang, 1997). Finally, the designs of two pilot-scale SMB processes for fructose purification are presented as examples of anti-Langmuir isotherm systems. Single component and competitive isotherms are determined from batch equilibrium tests. Mass-transfer parameters are estimated from pulse, breakthrough, and elution data obtained at different concentrations and flow rates. The flow rates and switching

time are calculated from the isotherms according to the standing wave analysis. Predicted steady-state column profiles and effluent product concentrations agree closely with the data obtained from two pilot-scale SMB systems.

Theory

In this section, the standing wave analysis is introduced for continuous moving bed (CMB) chromatography systems with nonlinear isotherms. Nonlinear wave velocities can be derived from batch elution data and can be used to determine the flow rates and switching time that are required for complete separation. The standing wave design gives the optimal flow rates and switching time for systems without mass-transfer effects.

Equations for CMB systems

Mass Balance for the Mobile Phase within a Zone. The transport equation for a solute in the mobile phase in zone I in CMB can be given as (Ma and Wang, 1997)

$$\frac{\partial c_{bi}}{\partial t} = E_{bi}^{\mathrm{I}}\frac{\partial^2 c_{bi}}{\partial x^2} - \bar{u}_0^{\mathrm{I}}\frac{\partial c_{bi}}{\partial x} - PK_{fi}^{\mathrm{I}}(c_{bi} - c_i^*) \quad i = 1, 2 \quad (1)$$

where c_{bi} and c_i^* are the mobile- and average-pore phase concentrations of the ith component, respectively. P is the bed-phase ratio, $(1-\epsilon_b)/\epsilon_b$, and ϵ_b is the interstitial void fraction. $\bar{u}_0^{\mathrm{I}}$ is the interstitial linear mobile-phase velocity along the axial direction (x). The sorbent movement velocity ν is along the $(-x)$ direction. The input and output ports remain stationary in this coordinate system. Equations for other zones are the same as Eq. 1 except that the values of E_b, K_f, and u_0 are different. For a fixed-bed or SMB system discussed later, the interstitial velocity relative to the sorbent phase u_0 is the velocity that controls the propagation of concentration waves relative to the sorbent phase. These two velocities are related by $u_0^{\mathrm{I}} = \bar{u}_0^{\mathrm{I}} + \nu$. Since this study has a major emphasis on SMB systems, $\bar{u}_0^{\mathrm{I}}$ in Eq. 1 is replaced by $u_0^{\mathrm{I}} - \nu$ in the following analysis.

Mass Balance for the Pore Phase within a Zone. The following equation for the lumped mass-transfer model is proposed for a CMB process. Corresponding equations for fixed-bed adsorption processes can be found in Santacesaria et al. (1982)

$$\epsilon_p\frac{\partial c_i^*}{\partial t} + (1-\epsilon_p)\frac{\partial q_i^*}{\partial t} = K_{fi}^{\mathrm{I}}(c_{bi} - c_i^*) + \nu\epsilon_p\frac{\partial c_i^*}{\partial x} + (1-\epsilon_p)\,\nu\frac{\partial q_i^*}{\partial x} \quad (2)$$

where q_i^* is the averaged solid-phase concentration. When local equilibrium is assumed, the competitive Langmuir equation (Eq. 7) is usually used to describe the relation between q_i^* and c_i^*. Equations 1 and 2 give the set of equations of the lumped rate model for CMB processes.

Equilibrium Model without Mass Transfer and Axial Mixing. Notice that for a binary system when E_{bi} approaches zero and in the absence of other mass-transfer effects, the following equations are obtained from Eqs. 1 and 2

$$(1+P\epsilon_p)\frac{\partial c_1}{\partial t} + (u_0 - \nu - P\epsilon_p\nu)\frac{\partial c_1}{\partial x} + P(1-\epsilon_p) \times\left[\left(\frac{\partial q_1}{\partial c_1} + \gamma^{-1}\frac{\partial q_1}{\partial c_2}\right)\frac{\partial c_1}{\partial t} - \nu\left(\frac{\partial q_1}{\partial c_1} + \gamma^{-1}\frac{\partial q_1}{\partial c_2}\right)\frac{\partial c_1}{\partial x}\right] = 0 \quad (3a)$$

$$(1+P\epsilon_p)\frac{\partial c_2}{\partial t} + (u_0 - \nu - P\epsilon_p\nu)\frac{\partial c_2}{\partial x} + P(1-\epsilon_p) \times\left[\left(\frac{\partial q_2}{\partial c_2} + \gamma\frac{\partial q_2}{\partial c_1}\right)\frac{\partial c_2}{\partial t} - \nu\left(\frac{\partial q_2}{\partial c_2} + \gamma\frac{\partial q_2}{\partial c_1}\right)\frac{\partial c_2}{\partial x}\right] = 0 \quad (3b)$$

The superscript I and subscript b are dropped for the sake of simplicity. Note γ is defined as Dc_1/Dc_2; the capital D is used to denote that the differential is based on an observer moving at a certain wave velocity (Eq. 4) associated with a specific concentration pair (c_1, c_2)

$$u_{si}(c_1, c_2) = \frac{u_0}{1 + P\epsilon_p + P(1-\epsilon_p)\left.\dfrac{Dq_i}{Dc_i}\right|_{c_1, c_2}} \quad i = 1, 2 \quad (4)$$

where

$$\frac{Dq_1}{Dc_1} \equiv \frac{\partial q_1}{\partial c_1} + \frac{\partial q_1}{\partial c_2}\gamma^{-1} \quad (5a)$$

$$\frac{Dq_2}{Dc_2} \equiv \frac{\partial q_2}{\partial c_2} + \frac{\partial q_2}{\partial c_1}\gamma \quad (5b)$$

Note also Eqs. 3a and 3b are different from those in the literature (Rhee et al., 1971); the mass balance equations (Eqs. 1 and 2) in this study are based on the absolute velocities of the solvent and that of the sorbent. The net linear velocity associated with a specific concentration pair with respect to the feed port in CMB can be expressed as

$$u_{wi}(c_1, c_2) \equiv u_{si}(c_1, c_2) - \nu \quad i = 1, 2 \quad (6)$$

For a system with a Langmuir isotherm

$$q_i = \frac{a_i c_i}{1 + \sum_1^2 b_i c_i} \quad i = 1, 2 \quad (7)$$

γ becomes a constant for large overlapping bands (Rhee et al., 1970, 1971) and can be found from the concentration diagram (c_1 vs. c_2, Figure 2d) called a hodograph as explained later. The following observations can be made from Eqs. 4–6 for CMB systems without mass-transfer resistances: (1) a concentration wavelet (concentration wave associated with a specific concentration or a pair of concentrations) can be kept standing if the flow rate is chosen such that $u_{wi} = 0$ in Eq. 6; (2) N different wavelets can be selectively made stationary if N zones with N different flow rates are used; and (3) the net concentration wave velocity is a function of two *independent* linear velocities: the solid movement velocity (a constant value) and the solute movement velocity (a concentration-dependent value) which can be determined from batch elution profiles as shown in the following sections.

Conditions to achieve standing concentration waves

In systems with linear isotherms and negligible mass-transfer resistances, there are only two waves (adsorption and desorption) for each solute band and they are independent of solute concentrations. In a binary SMB system, in order to obtain pure products, all four waves should be standing so that zone II contains only the fast migrating solute and zone III only the slow migrating solute (Ma and Wang, 1997). In contrast, in nonlinear systems, the solute migration velocity is concentration-dependent. There are three different concentration waves associated with each component. In order to apply the standing wave analysis, specific concentration wavelets have to be identified and made standing. This can be done by analyzing the batch elution effluent concentration histories of a wide feed pulse, which consists of a step increase in feed concentrations, constant concentrations, and a step decrease in concentrations (Ma and Guiochon, 1990a).

Standing Waves for Complete Separation at Output Ports. In a binary system, the elution of a large feed pulse results in the typical concentration column profiles and effluent histories shown in Figures 2 and 3 for a sufficiently long column. For a convex isotherm (Langmuir type), the column profiles generally show the pattern as in Figure 2a. There is a plateau region where only the low affinity solute is present, and its concentration (c_{p1}) exceeds its feed concentration. This plateau is in between two self-sharpening waves (6 and 5). There is a second plateau region (between 4 and 5 in Figure 2a) where both solutes are present and their concentrations

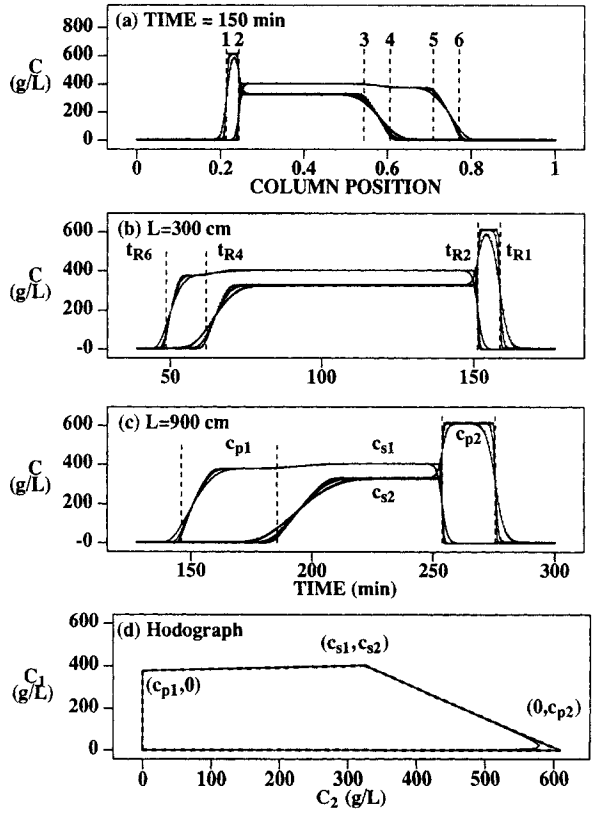

Figure 3. Similar plots as in Figure 2 for an anti-Langmuir isotherm system.

are the same as the feed concentrations ($c_{s1} = c_{f1}$, $c_{s2} = c_{f2}$). A diffuse wave region (between wavelets 3 and 4) is followed by a third plateau region where only the high affinity solute is present (c_{p2}). This plateau is again followed by a diffuse wave of the high affinity solute (between 1 and 2).

For an anti-Langmuir or concave isotherm ($b_1 < 0$, $b_2 < 0$), the concentration profiles (Figure 3a) differ from those in Figure 2a: two diffuse wave regions (between 5 and 6, and 3 and 4) are followed by a plateau and two self-sharpening waves (1 and 2) which are the boundaries of the plateau of the more retained compound.

In order to have continuous steady-state operation, the four zone flow rates have to satisfy the following conditions.

$$F^{\mathrm{I}} = F^{\mathrm{IV}} + F^{\mathrm{feed}} \tag{8}$$

$$F^{\mathrm{II}} = F^{\mathrm{I}} - F^{\mathrm{raff}} \tag{9}$$

$$F^{\mathrm{III}} = F^{\mathrm{II}} + F^{\mathrm{solv}} \tag{10}$$

$$F^{\mathrm{IV}} = F^{\mathrm{III}} - F^{\mathrm{extr}} \tag{11}$$

If the following four wavelets in Figure 2 are confined within the individual zones (wavelet 1 in zone III; wavelet 3 in zone IV; wavelet 5 in zone I; and wavelet 6 in zone II) complete separation at the extract and raffinate ports and pure products can be guaranteed. This corresponds to the following

$$u_{s5}^{\mathrm{I}} - \nu < 0 \tag{12a}$$

$$u_{s6}^{\mathrm{II}} - \nu < 0 \tag{13a}$$

$$u_{s1}^{\mathrm{III}} - \nu > 0 \tag{14a}$$

$$u_{s3}^{\mathrm{IV}} - \nu > 0 \tag{15a}$$

Equations 12a–15a define all the feasible flow rates and average port moving velocity that guarantee separation, that is, conditions such that wavelet 5 is kept away from the raffinate port, wavelets 1 and 6 are kept away from the solvent port, and wavelet 3 is kept away from the extract port.

Note that the boundary values of Eqs. 12a–15a are the following

$$u_{s5}^{\mathrm{I}} - \nu = 0 \tag{12b}$$

$$u_{s6}^{\mathrm{II}} - \nu = 0 \tag{13b}$$

$$u_{s1}^{\mathrm{III}} - \nu = 0 \tag{14b}$$

$$u_{s3}^{\mathrm{IV}} - \nu = 0 \tag{15b}$$

Equations 12b–15b correspond to the standing wave conditions. It is easily seen that the flow rates derived from the standing wave conditions give the highest feed flow and the lowest desorbent flow among all the flow rates that guarantee complete separation. In practice, the feed flow rate and column cross-sectional area are usually given. In this case the following must be satisfied

$$\frac{F^{\mathrm{feed}}}{\epsilon_b S} = u_0^{\mathrm{I}} - u_0^{\mathrm{IV}} \tag{16}$$

For the standing wave conditions there are five equations (Eqs. 12b–15b and 16); therefore, the five unknowns, which include the four interstitial velocities (u_0) and the sorbent movement velocity (ν), can be determined. Note any other design with flow rates that violate Eqs. 12a–15a cannot achieve complete separation. Any design with flow rates that satisfy Eqs. 12a–15a will require a smaller feed flow rate and consume more solvent than the standing wave design based on Eqs. 12b–15b and 16.

The wave migration velocities can be determined either from batch elution experiments or from isotherms obtained from other methods as explained below. For concave or anti-Langmuir isotherms (as in the fructose and glucose system introduced later in the experimental section), u^{I}_{s5} (Figure 2a) is substituted by u^{I}_{s4} (Figure 3a) and u^{III}_{s3} (Figure 2a) by u^{III}_{s2} (Figure 3a) in Eqs. 12–15.

Note that specific waves have to be identified and made standing in order to derive the optimal set of conditions for complete separation. Nonlinear wave analysis can be found in Rhee and Amundson (1971), Rhee et al. (1989), and Storti et al. (1989, 1993, 1995) for true countercurrent systems. However, these researchers did not identify the specific set of standing waves which give the optimal zone flow rates and switching time as discussed later in the results section.

Concentration Profiles in Batch Elution and the Hodograph Plot. In batch elution, column concentration profiles (Figures 2a and 3a) at a given time or effluent histories (Figures 2b, 2c, 3b, and 3c) at a given column length can be used to derive the wave migration velocities in Eqs. 12b–15b. In nonlinear systems the two solutes compete for adsorption sites and their concentrations are interdependent. Such dependence is determined only by the isotherm and the feed concentrations and can be found when the concentration profiles are plotted in the *hodograph plot* (Rhee et al., 1970, 1971, 1989; Ma et al., 1990b). In the absence of mass-transfer effects, the concentrations of the two solutes (Figures 2d and 3d) are linearly related. The two straight lines in the hodograph plot (Figure 2d) can be derived from the concentration profiles in Figure 2a by taking the axial distance as the implicit parameter or from effluent histories (Figure 2c) by taking the time as the implicit parameter. Note if the column is sufficiently long (compare Figures 2b and 2c), the hodograph plot is independent of column length and flow rate; it only depends on the feed concentrations and the isotherms (Figure 2d).

Since both c_1 and c_2 are linearly related, c_{p1} and c_{p2} can be determined from the following equations (Rhee et al., 1989; Ma et al., 1990b)

$$c_1 = \gamma_+ c_2 + A_+ \tag{17a}$$

$$c_1 = \gamma_- c_2 + A_- \tag{17b}$$

where

$$A_+ = \frac{a_1 - a_2}{a_2 b_1 + a_1 b_2/\gamma_+} \tag{18a}$$

$$A_- = \frac{a_1 - a_2}{a_2 b_1 + a_1 b_2/\gamma_-} \tag{18b}$$

Note when $c_2 = 0$, $c_1 = c_{p1}$, and when $c_1 = 0$, $c_2 = c_{p2}$ (Figure 2d). The γ_+ and γ_- are the roots of the following quadratic equation

$$\frac{\partial q_2}{\partial c_1}\gamma^2 + \left(\frac{\partial q_2}{\partial c_2} - \frac{\partial q_1}{\partial c_1}\right)\gamma - \frac{\partial q_1}{\partial c_2} = 0 \tag{19}$$

Equation 19 can be derived from Eq. 5 and the following equation

$$\frac{Dq_1}{Dc_1} = \frac{Dq_2}{Dc_2} \tag{20}$$

For competitive systems, Eq. 19 always has two real roots (Rhee et al., 1970, 1989). In batch elution the derivatives in Eq. 19 are evaluated at the feed concentrations (c_{f1}, c_{f2}) while in SMB systems the derivatives are evaluated at steady-state concentrations (c_{s1}, c_{s2}) at the feed position. In SMB the feed is diluted by the recycle stream. As a result, c_{s1} and c_{s2} are usually lower than c_{f1} and c_{f2} and they depend on the zone flow rates and port switching time.

Determination of Standing Waves. Once the isotherms are determined, the flow rates and the solid movement velocity in CMB (or the port switching time in SMB) can be derived as follows. In nonlinear systems, self-sharpening can occur at the leading front (or adsorption wave) of the migration bands for convex or Langmuir type isotherms (Figure 2a); or at the tail (or desorption wave) of the bands for concave or anti-Langmuir type isotherms (Figure 3a). When mass-transfer resistances are significant, the self-sharpening waves assume constant patterns (Figures 2a and 3a). When mass-transfer resistances are negligible, the self-sharpening waves become so sharp that concentration discontinuities (concentration shocks) occur. In either case, the migration velocity of a constant pattern wave or a shock wave is related to the concentration jump across the wave (Rhee et al., 1970). Note that in Figure 2a, waves 5 and 6 are constant pattern waves, and the terms Dq_1/Dc_1 and Dq_2/Dc_2 in Eq. 4 have to be substituted by the concentration jumps across the shocks $\Delta q_1/\Delta c_1$ and $\Delta q_2/\Delta c_2$, respectively. The wave velocities in Eqs. 12–15 can be determined from the following

$$u^{I}_{s5} = \frac{u^{I}_0}{1 + P\epsilon_p + P(1-\epsilon_p)\left.\dfrac{\Delta q_2}{\Delta c_2}\right|_{(c_{s1}, c_{s2})}} \tag{21a}$$

$$u^{II}_{s6} = \frac{u^{II}_0}{1 + P\epsilon_p + P(1-\epsilon_p)\left.\dfrac{\Delta q_1}{\Delta c_1}\right|_{(c_{p1}, 0)}} \tag{22a}$$

$$u^{III}_{s1} = \frac{u^{III}_0}{1 + P\epsilon_p + P(1-\epsilon_p)\left.\dfrac{Dq_2}{Dc_2}\right|_{(0,0)}} \tag{23a}$$

$$u^{IV}_{s3} = \frac{u^{IV}_0}{1 + P\epsilon_p + P(1-\epsilon_p)\left.\dfrac{Dq_1}{Dc_1}\right|_{(0, c_{p2})}} \tag{24a}$$

From Eqs. 12b, 15b, 16, 21a, and 24a, the average port movement velocity can be derived

$$v = \frac{F^{\text{feed}}}{S(1-\epsilon_b)(1-\epsilon_p)\left[\left.\frac{\Delta q_2}{\Delta c_2}\right|_{(c_{s1},c_{s2})} - \left.\frac{Dq_1}{Dc_1}\right|_{(0,c_{p2})}\right]} \tag{25a}$$

For anti-Langmuir isotherms

$$u_{s4}^{\text{I}} = \frac{u_0^{\text{I}}}{1+P\epsilon_p+P(1-\epsilon_p)\left.\frac{Dq_2}{Dc_2}\right|_{(c_{p1},0)}} \tag{21b}$$

$$u_{s6}^{\text{II}} = \frac{u_0^{\text{II}}}{1+P\epsilon_p+P(1-\epsilon_p)\left.\frac{Dq_1}{Dc_1}\right|_{(0,0)}} \tag{22b}$$

$$u_{s1}^{\text{III}} = \frac{u_0^{\text{III}}}{1+P\epsilon_p+P(1-\epsilon_p)\left.\frac{\Delta q_2}{\Delta c_2}\right|_{(0,c_{p2})}} \tag{23b}$$

$$u_{s2}^{\text{IV}} = \frac{u_0^{\text{IV}}}{1+P\epsilon_p+P(1-\epsilon_p)\left.\frac{\Delta q_1}{\Delta c_1}\right|_{(c_{s1},c_{s2})}} \tag{24b}$$

From Eqs. 12b, 15b, 16, 21b and 24b, the average port movement velocity can be derived

$$v = \frac{F^{\text{feed}}}{S(1-\epsilon_b)(1-\epsilon_p)\left[\left.\frac{Dq_2}{Dc_2}\right|_{(c_{p1},0)} - \left.\frac{\Delta q_1}{\Delta c_1}\right|_{(c_{s1},c_{s2})}\right]} \tag{25b}$$

Once the isotherms are known, the zone flow rates and the average bed moving velocity can be determined from Eqs. 12b–15b and 21a–25a for Langmuir isotherms, or from Eqs. 21b–25b for anti-Langmuir isotherms.

Note the hodograph plots are straight lines only for systems with Langmuir or anti-Langmuir isotherm equations (Eq. 7); for general convex or concave isotherms, a hodograph plot can also be used to determine the concentrations c_{p1} and c_{p2} for a given c_{s1} and c_{s2}. The hodograph plot can be correlated with nonlinear equations instead of Eq. 17 and 18 to decouple the interaction in the nonlinear isotherm equations.

Note in true countercurrent systems, the steady-state concentrations are the same as the feed concentrations. However, in SMB with four zones arranged as in Figure 1, the concentrations c_{s1} and c_{s2} are always less than those of the feed because the feed is diluted by the recycle stream of which the concentrations depend on zone flow rates and switching time. In this case the shock velocities calculated using the feed concentrations will be larger than those calculated using c_{s1} and c_{s2}. The velocity of wave 3 in Figure 2a, calculated based on the feed concentrations, will be slower than that calculated with lower concentrations. The velocity of wavelet 1 does not depend on the concentrations, because it corresponds to zero concentrations. This means the flow rates and switching time derived from Eqs. 21–25 using the feed concentrations to replace the unknown steady-state concentrations (c_{s1} and c_{s2}) satisfy the feasible conditions for complete separations defined in Eqs. 12a–15a. Similar argument can be made for anti-Langmuir systems.

The design based on the feed concentrations instead of the steady-state concentrations is not the optimal design, but it is close to the optimal design as shown in the result section. In order to find the optimal design, the following iterative procedure is proposed: (1) use the feed concentrations to calculate initial flow rates and switching time and perform simulations to get a set of c_{s1} and c_{s2}; (2) use the concentrations c_{s1} and c_{s2} to derive new zone flow rates and switching time, then perform numerical simulation to find a new set of c_{s1} and c_{s2}, and so on. As shown later in the result section (Table 3), this procedure converges easily and the optimal flow rates and switching time are highly dependent on the feed concentrations in nonlinear systems.

Derivation of Wave Velocities From Elution Profiles. From the analysis in the previous section, one can see that the wave velocities can be determined from the isotherms either obtained by the equilibrium test or from the elution chromatogram of a wide pulse. The wave velocities can also be determined directly from the experimental elution chromatogram as explained below.

In order to obtain the plateau in batch elution (Figures 2 and 3), relatively small particles are needed to reduce wave spreading. Usually, HPLC or medium pressure chromatography is used. In such systems, the linear velocities in Eqs. 12b–15b can be derived from the elution histories. There are two major advantages in using elution profiles for the determination of wave velocities: (1) the same feed in SMB can be used in batch elution experiments. In certain cases, even the same column, which will be used in SMB, can be used in batch elution experiments. For such cases, the batch results are less susceptible to errors caused by uncontrolled differences between batch and SMB experiments; and (2) data correlation or modeling of the competitive isotherm is relatively easy.

For each component, the portion of the isotherm which governs the elution process consists of only two curves which are the interception of the isotherm surface, for example, $q_1(c_1, c_2)$, with the two vertical planes which project onto the $c_1 - c_2$ plane as the two straight lines in the hodograph plot. The two curves can be determined easily from elution experiments using the hodograph plot. In case of a Langmuir isotherm, because the concentrations of the two solutes are linearly related, the multicomponent isotherm equation can be reduced to an effective single component equation. It is much easier to correlate the equilibrium data over this limited concentration range using the effective single component isotherm equation than using the competitive Langmuir isotherm equation.

For fixed concentrations, the denominator (retention factor) in Eq. 4 is constant and independent of u_0. The denominator can be determined from the retention time of a specific wavelet. Therefore, by identifying the retention times associated with the concentration pairs at the corners of the quadrilateral on the hodograph plot, one can derive the zone

flow rates from the following

$$u_{s5}^{\mathrm{I}} = \frac{u_0^{\mathrm{I}}}{1+P\delta^{\mathrm{I}}} \qquad P\delta^{\mathrm{I}} = \frac{t_{R5}-t_0}{t_0} \tag{26}$$

$$u_{s6}^{\mathrm{II}} = \frac{u_0^{\mathrm{II}}}{1+P\delta^{\mathrm{II}}} \qquad P\delta^{\mathrm{II}} = \frac{t_{R6}-t_0}{t_0} \tag{27}$$

$$u_{s1}^{\mathrm{III}} = \frac{u_0^{\mathrm{III}}}{1+P\delta^{\mathrm{III}}} \qquad P\delta^{\mathrm{III}} = \frac{t_{R1}-t_0}{t_0} \tag{28}$$

$$u_{s3}^{\mathrm{IV}} = \frac{u_0^{\mathrm{IV}}}{1+P\delta^{\mathrm{IV}}} \qquad P\delta^{\mathrm{IV}} = \frac{t_{R3}-t_0}{t_0} \tag{29}$$

where t_{Ri} is the retention time of wavelet i and t_0 is the dead time (the retention time of a large nonadsorbing species that is excluded from all the pores). For a Langmuir isotherm at low concentration, $\delta = \epsilon_p + (1-\epsilon_p)a$. Note the retention time of the adsorption waves is the elapsed time between the breakthrough and step up. For desorption waves, the retention times are determined from the time of step down in concentration at the inlet. The average port movement velocity can be found as follows

$$v = \frac{F^{\text{feed}}}{S(1-\epsilon_b)(1-\epsilon_p)(\delta^{\mathrm{I}}-\delta^{\mathrm{IV}})} \tag{30}$$

The zone flow rates can then be determined using Eqs. 26–29 and 12b–15b. Similarly, the zone flow rates can be determined from elution experiments for an isothermal anti-Langmuir system, for which t_{R5} (Figure 2b) is substituted by t_{R4} (Figure 3b) and t_{R3} (Figure 2b) by t_{R2} (Figure 3b).

Method of numerical simulation and correlations

The numerical simulations were performed using an algorithm for SMB systems, which has been described in detail in a previous article (Ma and Wang, 1997). The algorithm is based on periodic port movement in a ring of fixed beds. It can be used to simulate both CMB and SMB systems. The method of orthogonal collocation on finite elements (OCFE) (Ma and Guiochon, 1991) was used to solve the mass balance equations.

The lumped mass-transfer coefficient (K_f) can be estimated either from correlations or from best fitting of experimental elution data. For linear isotherm systems, it can also be estimated from the pore diffusion coefficient (D_p) and film mass-transfer coefficient (k_f) through the following equation (Ma and Wang, 1997; Ma et al., 1996)

$$\frac{1}{K_f} = \frac{R^2}{15\epsilon_p D_p} + \frac{R}{3k_f} \tag{31}$$

Similar equations can be found in Glueckauf (1955) and Santacesaria et al. (1982). D_p can be found from pulse elution or estimated from Brownian diffusivity using the correlation of Mackie and Meares (1955); k_f can be found from the correlation of Wilson and Geankoplis (1966). The E_b in Eq. 1 can be found from the correlation of Chung and Wen (1968) or estimated from experimental data.

Experimental Studies

Materials

Solutions for the batch equilibrium and pulse tests were made from reagent grade fructose and glucose from Sigma and deionized water, which were mixed in various ratios to obtain the desired concentrations. The feed solution used in the ADSEP SMB pilot testing was commercially available 42 high fructose corn syrup (HFCS). The composition of the feed was 42.5 wt.% fructose, 52.9% glucose, 4.6% polysaccharides. The feed contained 59.9% dissolved dry solid.

The adsorbent used for this study was U.S. Filter SM-49, a strong-acid cation exchange resin in the calcium form. The resin matrix is a sulfonated 5.5% cross-linked styrene/DVB copolymer. This type of resin has been used extensively by the corn sweetener industry for the fractionation of glucose and fructose (Corbett and Burke, 1996). The average particle diameter was 325 μm. The density of the hydrated calcium-form resin was 1.30 g/mL and moisture content was 47% by weight, which can be translated to a particle porosity of about 60%. The bed porosity was measured as 0.35.

Analytical

Sugar concentrations were measured using refractometry and High-Performance Liquid Chromatography (HPLC) analysis. A Milton Roy refractometer was used to measure total dissolved solids by comparing refractive index to calibration data tables. Waters HPLC was used to measure the ratio of the sugars. The HPLC used a 300×7.8 mm Bio-Rad Aminex HPX-87C column to separate the sugars. Injection volume was 20 μL. The peaks were detected by a Waters differential refractometer. The ratio of sugars to total solids was based on area percent.

Batch equilibrium tests

The method for determining the equilibrium isotherms involves performing numerous batch equilibration tests using a wide range of solution concentrations. The experiments were chosen to test the interactions of all the components at concentrations encountered in commercial separations. The sugar concentrations in these tests ranged from zero to greater than the feed concentrations. Solutions were prepared from deionized water and reagent grade chemicals. Each test used a known volume of solution (50 mL) with a known volume of hydrated resin (50 g). By measuring the sugar concentrations of the solution before and after the equilibration, it was possible to determine the sugar concentrations in the resin phase and calculate the equilibrium constant.

The interstitial water was removed from a large quantity of resin by placing the resin in a Buchner funnel and drawing moist air through the resin with vacuum. Moist air is used to prevent evaporation of water held in the intraparticle pore. Several batches were prepared to perform all of the tests. The resin was mixed well to assure uniformity. A known weight of resin was placed in an equilibration jar at room temperature. The volume of the resin (V_p) was calculated from the weight and density.

A known volume of solution (V_s) was added to the equilibration jar at room temperature. The jars were sealed to prevent evaporation and placed in a 65°C shaker bath for one hour. Afterward, the solution from the jar was separated from the resin while still at the equilibration temperature (65°C). Both the initial and equilibrium solutions were sampled and analyzed for sugar concentration.

The resin concentration (based on per solid volume) for each component was calculated by the following equation

$$q_s = \frac{V_s(c_{0i} - c_{fi}) - K_e \epsilon_p V_p c_{fi}}{(1 - K_e \epsilon_p) V_p} \tag{32}$$

where ϵ_p is the pore void and K_e is the fraction of the pore volume accessible to the sugars. In this case the K_e value is found to be 0.42; greater values result in negative q_s values.

Pulse tests

A vertically mounted 6 in.×3 in. diameter jacketed pyrex column was used for the pulse tests. The column bottom held a porous polypropylene disk to support the resin and a 1/4 in. (6.4 mm) needle valve to manually control the flow rate. The column top was designed to allow the feed distributor to be positioned for various bed depths. The placement of the feed distributor was made variable by incorporating a teflon ferrule with a bored-through fitting. The eluent could be directed either through the distributor or through the top of the column by opening and closing valves. The column top was also equipped with a vent valve and pressure gauge. The feed solution and eluent were stored in pyrex reservoirs. Both liquids were pumped with magnetically driven plastic gear pumps. The apparatus was used for the breakthrough and elution curves, as well as the pulse tests.

Resin loading was accomplished by removing the column top and adding a water slurry of the resin to the column. The resin was settled by backwashing the resin and allowing it to settle by gravity. After reattaching the top, the column was purged of air, and the adsorbent was rinsed with degassed water. The column was then heated to 150°F (66°C). Several washing cycles with sugar solution and water were performed to further settle the bed and the distributor was placed approximately 1/2 in. (12.7 mm) above the packings.

The feed solutions for the pulse tests were made from reagent grade glucose and deionized water. Various compositions, including single sugar solutions, were tested during this study. Flow rates and pulse sizes were also varied. At the start of a pulse test, the valves were adjusted to allow feed to flow through the distributor. At the same time, the column effluent was collected in a graduated cylinder. Because of its greater density, the feed quickly filled the space between the distributor and the separation media, and a sharp interface was formed between the feed solution and solvent at the level of the distributor. The volume of this 1/2 in. (12.7 mm) mixing space was approximately 60 mL or 1% of a bed volume. The remainder of the feed would have been pumped through the bed. After a set volume of effluent had been collected, which should have been the same as the volume of feed pumped into the column, the valves were switched to pump water through the distributor. When dilution lines appeared at the distributor, the valves were switched to pump the water into the top of the column, which pushed the remaining feed through the column from above. Samples were collected after a predetermined volume of effluent was collected in a graduated cylinder. The samples were analyzed and the sugar concentrations were tabulated vs. throughput. Volume throughput for each sample is based on the total volume collected from the start of the pulse test and the volumetric center of each composite sample. Sample size was 0.04 bed volumes.

During the pulse tests, particularly when using high concentration syrups, it was possible to visually monitor the sugars as they move through the column, because the gel resin changes color when in contact with the syrup. Therefore, it was possible to observe if plug flow was maintained. Usually, the loading portion of the pulse had good flow, while the washing portion showed some viscous fingering. At 150°F (66°C), the viscosity of water is 0.4 centipoise, while the viscosity of a 50% DS syrup is 2.7 cp. At high syrup concentrations, "fingers" as long as 1 ft (0.3 m) were observed in the resin bed. The viscous fingering results in a larger E_b value for desorption waves as explained in the results section.

Pilot SMB tests

A 6-in.-diameter ADSEP pilot plant was used for this portion of the study. The pilot plant consists of 12 stacked stainless steel sections as shown in Figure 1a. The feed and desorbent streams are continuously pumped into the system, while the extract and raffinate are continuously removed from the column. The recycle pump also runs continuously, but the output varies to control the four zone flow rates.

Details of the column sections are presented in Figure 1b. Each section has three inlet and two outlet valves connected to a common header and distributor which have a combined volume of 30 mL. This volume represents a possible route of cross contamination for the four process streams: feed, extract, desorbent, and raffinate (the fifth valve is for the flush stream, which is described below). Without using a flush, at the start of each step, the first 30 mL of feed added to the column is raffinate; the first 30 mL of extract removed is actually feed; the first 30 mL of desorbent added to the column is product; and the first 30 mL of raffinate removed is water. The flush is an optional step which is used in high purity applications to prevent feed from contaminating the extract by rinsing the header and distributor with water at the same flow rate as the feed at the end of each feed step. Thus, the first 30 mL of extract removed is water instead of feed. The flush does not prevent any of the other cross contaminations. For this study, the flush step was not used.

Each section holds 23.25 in. (590 mm) of resin and 1 in. (25.4 mm) of garnet to prevent the adsorbent from plugging the support screen. The sections are separated by 1-1/8 in. (28.6 mm) spacers, which hold two 1/8 in. (3.2 mm) screened distribution plates, creating a 7/8 in. (22.2 mm) void space. The spacers and the separation columns have the same internal diameter. The garnet is not believed to adsorb the sugars, but it does have a bed porosity of approximately 0.40. The recycle line between the bottom of section 12 and the top of section 1 and the recycle pump represent an excess dead volume of 1.14 L.

The resin is loaded as a slurry under 50 psi pressure. There is no void space between the top of the bed and the top resin support screen when the bed is filled with water. Although it has been shown that the resin shrinkage when in contact with concentrated syrups has been observed in the fixed-bed experiments, the formation of a void space in the ADSEP pilot plant has not been directly observed because of the construction of the pilot plant.

All valve switching and flow control on the pilot plant is automatic. Composite samples covering 2 h of operation were taken on a continuous basis to monitor the compositions of the extract and raffinate streams. Steady-state operation was assumed when similar sample compositions were obtained for three consecutive sets of samples. Separation profiles were generated by taking drip samples at one point from the recycle stream throughout one cycle. Each sample represents the average composition over one cycle.

In addition to the tests on the ADSEP system, tests were also done on a smaller system (MiniADSEP), which consists of eight individual columns [about 1 in. × 40 in. (25 mm × 1,016 mm)]. The columns were connected with tubings, and in between two columns there is a rotary valve to select the stream into or out of the circulation. Each column has, instead of the flow distributor, screens at the top and the bottom. The column packing and experimental testing procedure are similar to those used in the ADSEP system. There is a single sampling port to collect data of column profiles. The samples for column profiles were taken at the beginning and at the middle of each cycle.

Simulation Results and Discussion

In this section, simulation results for both elution and SMB systems are presented. The simulation parameters from the pilot-scale SMBs were used. The retention times of batch elutions (Figures 2b and 2c; Figures 3b and 3c) obtained from the simulation are compared with those obtained from Eqs. 4 to 7. Simulations are used to check the performance of SMB designs based on the flow rates and switching time calculated from Eqs. 12b–15b and 21b–25b. Note these equations derived in this study are based on the assumptions that mass-transfer resistances are negligible.

Profiles and effluent history in elution chromatography

Figure 2 shows the concentration profiles and effluent histories in batch elution. The dashed lines mark the retention times calculated from the equilibrium theories Eqs. 4 and 5 (Figure 2a). Simulation results obtained with three different particle sizes ($R = 25$, 50, and 100 μm, the largest particle size results in most dispersed bands) are shown as solid lines. As the particle size decreases, the simulation results approach the theoretical values indicated by the dashed lines. Note the calculated values are in the center of the constant pattern waves (position 5 and 6 in Figure 2a), whereas for the diffuse waves the calculated positions are ahead of the simulated position for the large particle case ($R = 100$ μm) because of significant spreading due to mass-transfer effects. When the particle size is reduced to 50 μm, the simulated retention times approach the calculated values. Figures 2b and 2c show that when the column length is sufficiently long

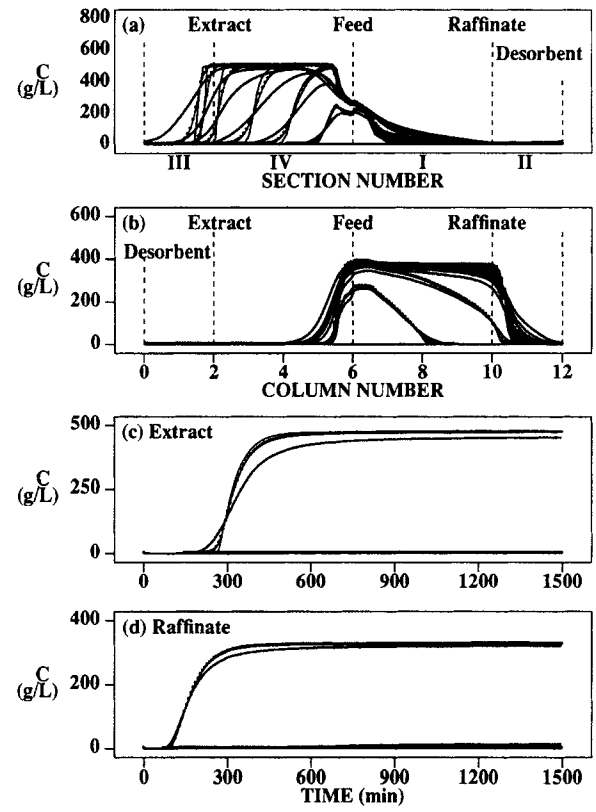

Figure 4. Simulated SMB profiles and effluent histories using the flow rates and switching time derived from Eqs. 21b and 25b with the feed concentrations.

Thin lines: $d_p = 80$ μm; dotted lines: $d_p = 160$ μm; thick lines: $d_p = 320$ μm. Other parameters are listed in Table 2: (a) transient column profiles for the more retained component obtained starting at 45 min and 82 min intervals for the next four profiles; the last profile obtained at 1,035 min.; (b) transient column profiles for the less retained component; (c) effluent history at extract port; (d) effluent history at raffinate port.

mass-transfer effects on the hodograph plot disappear. Similar behavior can be observed in Figure 3 for an anti-Langmuir system.

Profiles and effluent history in SMB systems

Mass-Transfer Effects. Figure 4 shows the simulation results for an SMB system. The flow rates and switching time are derived using Eqs. 21b–25b. The parameters are listed in Table 2. The profiles are obtained starting at 45 min and every 82 min for the next four curves, and at 1,035 min for the last curve. Three sets of mass-transfer parameters corresponding to particle sizes $d_p = 80$, 160, and 320 μm are used for the simulations. Over 99.9% pure products at both extract and raffinate ports are obtained for the particle sizes less than 320 μm. By observing the concentration profiles, one can see that if the particle size is sufficiently small or if the zone length is sufficiently long, relatively pure products can be obtained with the zone flow rates and port switching time derived from the equilibrium analysis. In other words, the mass-transfer effects can be reduced by the following: (1)

Table 2. System and Numerical Parameters for Figure 4*

Single Column	R (μm) 40,80,160	L_c (cm) 63.5	ϵ_b 0.402	ϵ_p 0.25	ID (cm) 16.15
SMB Systems		Zone I	Zone II	Zone III	Zone IV
	L (cm)	254	127	127	254
	F_r (cm^3/min)	1,173.5	922.93	1,110.2	972.48
$R = 40$ μm	E_b (cm^2/min)	0.2254	0.1776	0.2134	0.1822
	K_f (l/min)	18.317	18.195	18.290	18.223
$R = 80$ μm	E_b (cm^2/min)	0.4479	0.3532	0.4240	0.3719
	K_f (l/min)	4.6567	4.6316	4.6511	4.6373
$R = 160$ μm	E_b (cm^2/min)	0.8878	0.7006	0.8406	0.7377
	K_f (l/min)	1.1800	1.1749	1.1789	1.1760
Numerical Simulation	Elements 240	Colloc. 3	Δt 0.02 min	Switching Time 8.3691 min	

*Feed concentrations and isotherm parameters are the same as in Table 6.

decrease the particle size for a fixed zone length; or (2) increase the zone lengths for a fixed particle size. Figures 4c and 4d show the effluent concentration histories for the extract and raffinate, respectively. The concentrations are averaged over a cycle. Note that the averaged concentrations at steady state ($t > 1{,}500$ min) with large particles are lower than those with small particles, indicating that mass-transfer resistances affect the steady-state concentrations. When steady state is reached, the total rate of output equals that of input for each component. If the more retained solute has nonzero concentration at the raffinate port due to band spreading, its extract concentration has to be lower than that for small particles for which the raffinate concentration of the more retained solute is zero.

Figures 5 and 6 compare the simulation results for a CMB system with those for a corresponding SMB system (Figure 4) at two different particle sizes. The CMB simulations use 1,200 divisions to simulate the continuous movement of the bed. In the SMB system with small particles (80 μm) the waves are sharp and contained within one column (Figure 5). When the feed and desorbent ports are moved from one column to the next, waves are interrupted, causing the local concentration to increase near the feed port and to decrease near the desorbent port. Such discontinuities in concentration sharpen the column profiles. In CMB, the bed movement is continuous and sharpening due to the interruption is more pronounced, resulting in sharper column profiles than those in SMB (Figure 5). In the system with large particles (320 μm, Figure 6), the profiles are already dispersed and the sharpening caused by port switching is not as pronounced as in the small particle system (Figure 5). The results indicate that for large particle systems, CMB and SMB column profiles and effluent histories are almost identical (Figure 6). Therefore, the design criteria derived from the CMB can be applied to SMB. For the small particle systems, CMB column profiles and transient histories are significantly sharper than those for SMB. However, the product concentrations and purities at cyclic steady state are similar to those for SMB. These results suggest that, even for large particle systems, the design criteria derived from CMB can be used to design SMB and obtain similar product concentrations and purities at steady state.

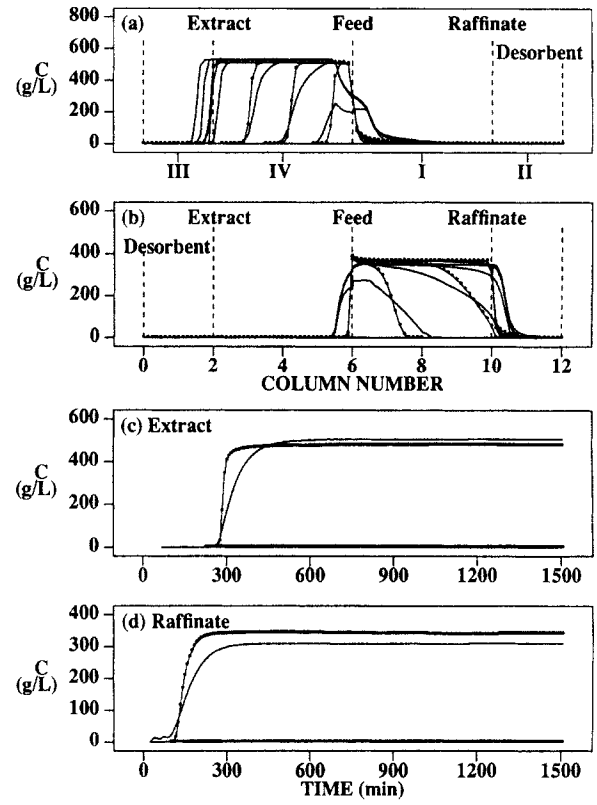

Figure 5. Simulated profiles and effluent histories based on the flow rates in Figure 4 for a CMB system (line with dots) and an SMB (thin lines) with $d_p = 80$ μm.

The same parameters and figure convention as in Figure 4 are used except $L_c = 0.635$ cm, $t_s = 0.083691$ min for the CMB case.

Flow Rate Effects. Figure 7 shows the simulation results obtained with 2.5% increase of the flow rates in zones I and II and 2.5% decrease in zones III and IV with respect to the values used in Figure 4; the switching time remains the same. Instead of near complete separation at the output ports as in Figure 4, the minor component breakthrough occurs at about 1,200 min for the extract and 800 min for the raffinate, resulting in impure extract and raffinate products at steady state. This result shows that if the flow rates deviate from the values for the standing wave design and violate Eqs. 12a–15a, pure products cannot be obtained.

By contrast, when the flow rates in zones I and II are decreased by 2.5% and those in zones III and IV are increased by 2.5% of the values for the standing wave design (Figure 4) and they satisfy Eqs. 12a–15a, better separations are obtained (profiles are similar to those in Figure 4 and they are not shown), especially in the large particle case. The improvements of the product purities are: (1) ($d_p = 80$ μm) raffinate from 99.92% to 99.99%, extract from 99.99% to 100.00%; (2) ($d_p = 320$ μm) raffinate from 95.37% to 97.44%, extract from 98.74% to 99.86%, but the product concentrations decrease. This result indicates that as the zone flow rates defined in Eqs. 12a–15a move away from the standing wave design values obtained from Eqs. 12b–15b, the purities are

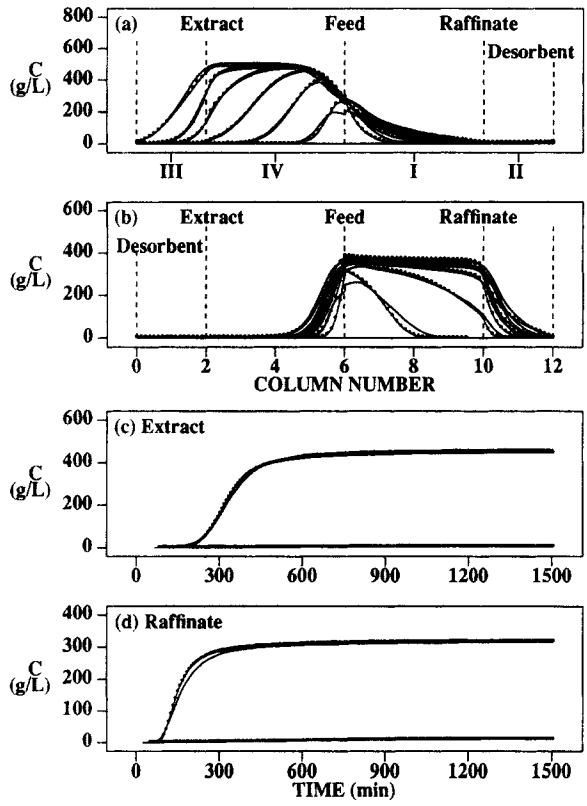

Figure 6. Simulated profiles and effluent histories based on the flow rates same as in Figure 4 for a CMB and an SMB system with $d_p = 320$ μm.

The convention and parameters are the same as in Figure 5.

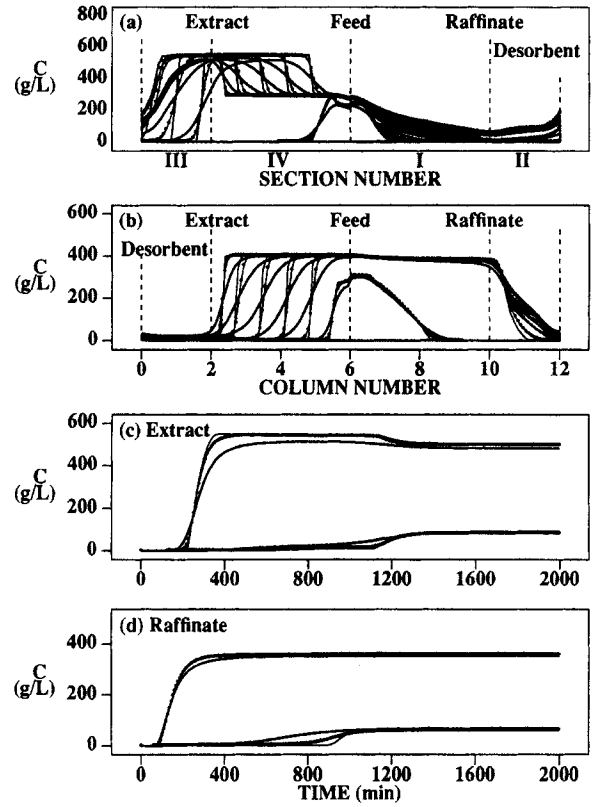

Figure 7. Simulated profiles and effluent histories based on the flow rates that violate Eqs. 12a–15a.

Parameters and the figure legends are the same as in Figure 4 except that the flow rates are increased by 2.5% for zones I and II and decreased by 2.5% for zones III and IV.

higher but the products are more diluted. This result also suggests that the standing wave design based on Eqs. 12b–15b and 21b–25b gives the maximum feed and minimum desorbent flow rates that guarantee complete separations.

Optimal Flow Rates and Steady-State Concentrations. As indicated previously, when mass-transfer resistances are negligible and the steady-state concentrations are known, flow rates and switching time determined from Eqs. 21–25 give the minimal desorbent flow rate for the given feed flow rate. However, the steady-state concentrations are unknown *a priori*. The optimal zone flow rates and switching time have to be determined through the iterative procedure introduced previously.

Figure 8 shows the dependence of flow rates on the steady-state concentrations at a fixed feed flow rate for a Langmuir (Figures 8a and 8b) and an anti-Langmuir system (Figures 8c and 8d). The isotherm parameters for Figure 2 are used for the Langmuir system and those for Figure 3 are used for the anti-Langmuir system. Identical concentrations for the two solutes are used. The optimal zone flow rates obtained from the iterative procedure increase with increasing feed concentrations for the Langmuir system (Figure 8a). The higher the feed concentrations, the higher the wave velocities for waves 3, 5 and 6 (Figure 2a). Equations 12b–15b show that the increase in wave velocities results in the increase in ν and the increase in the zone flow rates. The increasing zone flow rates with increasing c_{f1} results in the increases in the flow rates of desorbent, raffinate, and extract (Figure 8b). The optimal values (solid lines) are lower than the values calculated from Eqs. 12b–15b and 16 based on the feed concentrations c_{f1} and c_{f2} (dashed lines). This result means that the latter approach gives a more conservative design, which approaches the optimal design as the feed concentrations decrease.

For an anti-Langmuir system, the zone flow rates decrease with increasing feed concentrations (Figure 8c), because the wave velocities of waves 1, 2, and 4 decrease with increasing feed concentrations. Note the extract flow rate is the difference between the flow rate in zone III and flow rate in zone IV. Figure 8c shows the difference decreases with increasing feed concentrations, which causes a decrease in extract flow rate (Figure 8d). By contrast, the raffinate flow rate increases with increasing feed concentrations. Although the optimal flow rates decrease with increasing feed concentrations in the anti-Langmuir system, the zone flow rate calculated from Eqs. 12b–15b and 16 (modified for the anti-Langmuir isotherm) based on the feed concentrations c_{f1} and c_{f2} instead of c_{s1} and c_{s2} is more conservative than the optimal.

In both cases (Figure 8), the flow rates and port switching time calculated from Eqs. 12b–15b based on the feed concentrations (without iteration) are very close to the optimal values and are within the feasible domain defined by Eqs. 12a–15a. The results in Figure 8 also suggest that if the satu-

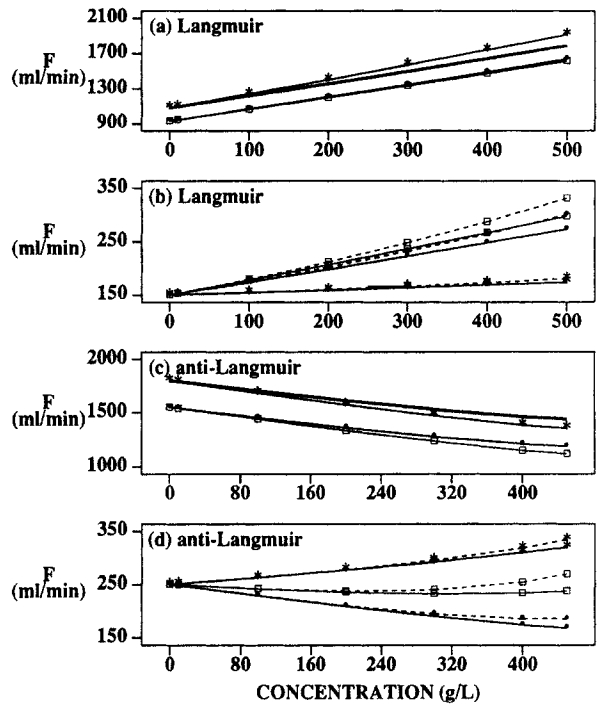

Figure 8. Dependence of optimal flow rates on the feed concentrations.

The values of c_{s1} and c_{s2} and the optimal step time and flow rates are listed in Table 3. The isotherm parameters are listed in Table 4. (a) Optimal zone flow rates as a function of c_{f1} ($c_{f1} = c_{f2}$), Zone I: solid line, Zone II: line with squares, Zone III: line with stars, Zone IV: line with dots; (b) desorbent (squares), raffinate (stars), and extract (dots) flow rates as a function of c_{f1}. The solid lines are obtained from the iterative procedure, whereas the dashed lines are calculated from Eqs. 12b–15b and Eq. 16 based on c_{f1} and c_{f2}; (c) optimal zone flow rates as a function of c_{f1} for an anti-Langmuir system. The convention follows that in Figure 8a; (d) desorbent, raffinate, and extract flow rates as a function of c_{f1}. The convention follows that in Figure 8b.

ration capacities are used as in Storti et al. (1989, 1995), the zone flow rates thus obtained would be more conservative and further away from the optimal (solid lines) than the standing wave design based on the feed concentrations (dashed lines).

In practice, the optimal values deviate from those obtained from Eqs. 12b and 15b. Such deviation is caused by two factors: (1) the optimal flow rates depend on the steady-state concentrations at the feed port which are unknown; (2) mixing effects due to mass-transfer resistances or extra-column dispersion. The former can be taken care of by the equilibrium analysis and the aforementioned iterative procedure. The latter has to be dealt with by using simulations as explained later.

Experimental Results and Discussion

As discussed in the theory section, in order to determine the flow rates and switching time for an SMB system, the isotherms and the mass-transfer parameters have to be determined. In the following, we apply the design method to two pilot processes for the separation of fructose from glucose. In order to test the robustness of the method introduced here, independent batch equilibrium tests were used to obtain the isotherms. Pulse and breakthroughs over a wide range of concentrations were used to estimate K_f and E_b, which are needed for simulations.

Batch tests

Figure 9 shows the isotherm data obtained for fructose and glucose. The data can be correlated with the multicomponent Langmuir isotherm equation with negative b values (Eq. 8) (anti-Langmuir isotherm). The parameters are listed in Table 4. Both single component (Figure 9a) and competitive (Figures 9b and 9c) batch tests were done. The data were correlated using the SYSNLIN procedure which treats multiobjective multivariant nonlinear systems in SAS. Figure 9b shows the isotherms of fructose at three different ranges of glucose concentrations (Triangles: 42–50 g/L, Squares: 80–90 g/L, Circles: 160–170 g/L). Figure 9c shows the isotherms of glucose at three different ranges of fructose concentrations (Triangles: 37–47 g/L, Squares: 74–80 g/L, Circles: 140–150 g/L). The anti-Langmuir equation correlates the data well

Table 3. Optimal Steady-State Concentrations and Flow Rates

		Langmuir		
C_{f1}, C_{f2} (C_{s1}, C_{s2})	Step Time	Desorbent	Raffinate	Extract
10,10(9.84,9.78)	8.165(8.167)	152.83(152.79)	150.41(150.41)	152.42(152.38)
100,100(95.10,96.61)	7.169(7.214)	179.57(178.20)	154.47(154.24)	175.11(174.96)
200,200(183.79,190.17)	6.250(6.375)	212.11(207.07)	159.75(158.80)	202.35(198.27)
300,300(269.26,282.51)	5.482(5.701)	247.93(236.58)	165.86(163.64)	232.08(222.94)
400,400(347.32,367.82)	4.829(5.173)	287.46(266.80)	172.81(168.76)	264.65(248.04)
500,500(422.01,450.17)	4.269(4.683)	331.22(297.70)	180.68(174.09)	300.54(273.61)
		Anti-Langmuir		
C_{f1}, C_{f2} (C_{s1}, C_{s2})	Step Time	Desorbent	Raffinate	Extract
10,10(9.84,9.76)	5.010(5.009)	249.07(249.07)	251.25(251.22)	247.82(247.86)
100,100(98.58,94.99)	5.361(5.356)	241.90(241.49)	262.96(262.57)	228.94(228.92)
200,200(197.05,182.86)	5.776(5.776)	237.54(235.29)	277.49(276.25)	210.05(209.04)
300,300(296.68,259.39)	6.190(6.225)	239.64(232.37)	294.90(291.67)	194.75(190.70)
400,400(393.19,322.50)	6.529(6.688)	253.96(233.61)	318.13(309.76)	185.83(173.85)
450,450(437.06,348.74)	6.623(6.873)	269.51(237.49)	333.98(319.54)	185.53(167.95)

The top half of the table is for the Langmuir system in Figures 8a and 8b, while the bottom half of the table is for the anti-Langmuir system in Figures 8c and 8d. The values of flow rates and step time obtained from Eqs. 12b and 15b based on c_{f1} and c_{f2} are listed, whereas the optimal values are in the parentheses. Particle diameter is 125 μm and 100% purity and recovery of each component are obtained. Results with 80 μm particles are similar to those listed indicating that the mass-transfer effects on the recovery and purity, as well as final steady-state concentrations, are negligible in the system. The same isotherm parameters as listed in Table 4 are used. The results are obtained with 2,000 min runs.

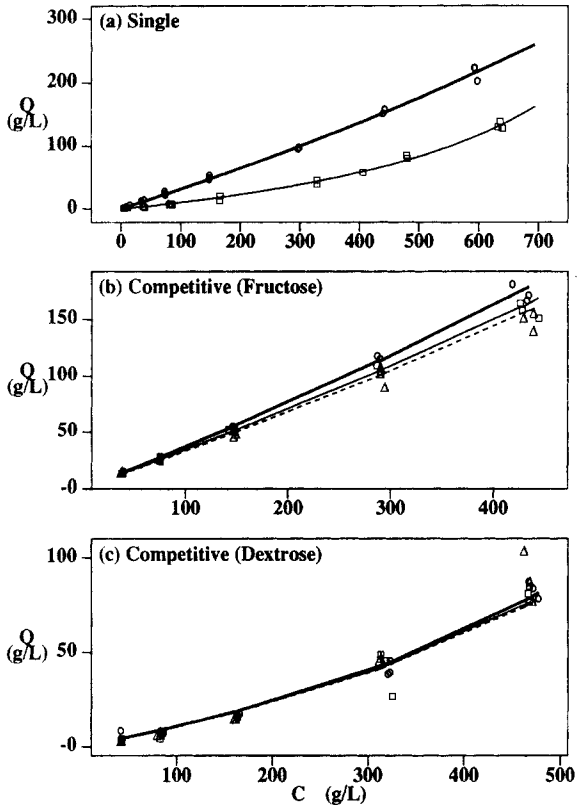

Figure 9. Isotherms for fructose and glucose obtained from batch equilibrium tests.

Correlated isotherm parameters and experimental parameters are listed in Table 4.

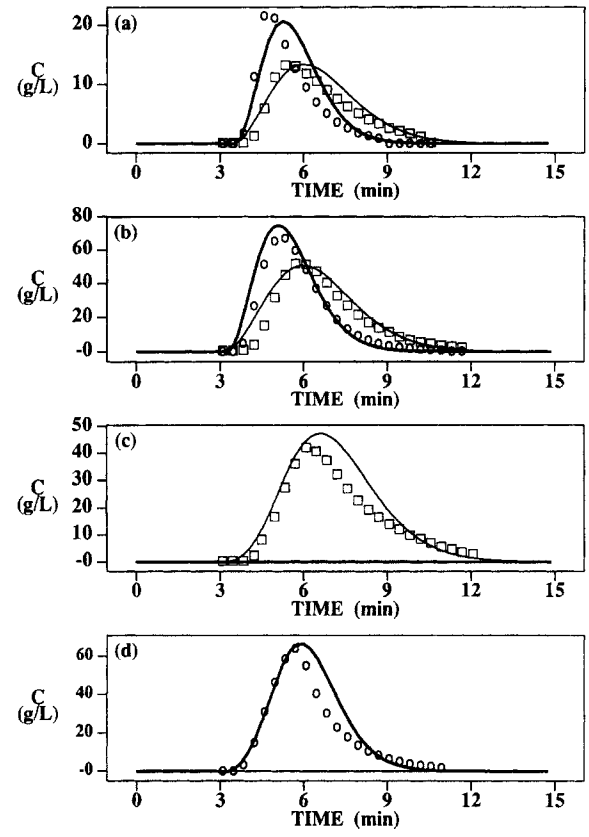

Figure 10. Four different pulse elution tests for fructose and glucose.

The simulation parameters are listed in Table 4.

for the single component data, but only reasonably well for the competitive data. The anti-Langmuir correlation underpredicts the interference between the two components.

Table 4. System Parameters for Figures 10c and 11

Column	L (cm)	F_r (mL/min)	ϵ_b	ϵ_p	ID (cm)	R (μm)
Fig. 10c	152.4	743.18	0.35	0.25	7.62	162.5
Fig. 11a,d	152.4	743.18	0.35	0.25	7.62	162.5
Fig. 11b,c	152.4	464.50	0.35	0.25	7.62	162.5

Comp. No.	E_b (cm^2/min)	K_f (l/min)	Isotherm a	Isotherm b
1	2.511	1.168	0.0948	-8.585×10^{-4}
2	2.511	1.168	0.3073	-2.540×10^{-4}

Fig. 10	C_{f1} (g/L) (Glucose)	C_{f2} (g/L) (Fructose)	Injection (min)
(a)	106.5	103.2	0.4676
(b)	402.5	407.6	0.4676
(c)	0.0	99.5	1.8703
(d)	101.9	0.0	1.8703

Fig. 11	C_{f1} (g/L)	C_{f2} (g/L)	Step Change (min)
(a)	0.0	516	0.0 (step up)
(b)	0.0	520	0.0 (step up)
(c)	490.0	0.0	0.0 (step down)
(d)	490.0	0.0	0.0 (step down)

Pulse and breakthrough tests

In order to estimate the mass-transfer parameters K_f, both pulse and breakthrough tests were performed on the 1 in. diameter column. E_b was estimated from the literature correlation by Chung and Wen (1968). The K_f values are then determined from the best fit of four sets of pulse data and two sets of breakthrough data. Figure 10 shows the comparison between the data and the simulation results for the pulse experiments. Figure 11 shows the breakthrough and wash experiments. In Figures 11c and 11d, the simulations for the washing experiments (thick line) do not agree with the data as well as those for the breakthroughs (Figures 11a and 11b). The simulated washing curves are less spread than the data. This can be attributed to the observed viscous fingering resulting from displacing a more viscous sugar solution with a less viscous desorbent (water). If E_b is increased by using an empirical correlation $E_b = 2.2\ u_0$, the agreement between simulations and the washing data is improved (thin lines in Figures 11c and 11d). The results show that such fingering effects on the desorption waves can be accounted for by the empirical correlation. As shown in a previous study, a similar correlation was used successfully to take into account dispersion due to nonuniform flow or extra-column mixing (Ma and Wang, 1997).

SMB experiments and comparison with simulations

For the MiniADSEP system, a feed flow rate is set to 5.9 mL/min. This feed flow rate and the isotherms from batch

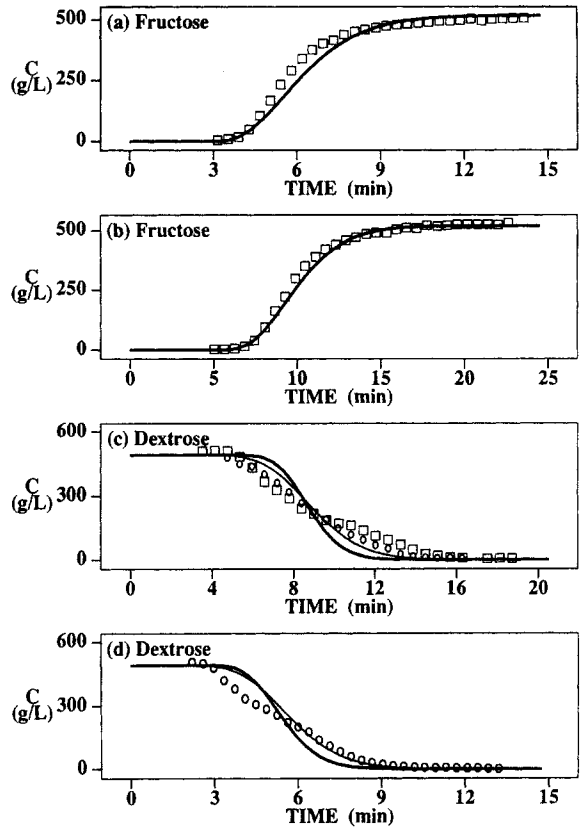

Figure 11. Elution data from four different breakthrough and washing experiments (symbols) compared with simulations (thick lines).

The same simulation parameters are listed in Table 4. The thin lines in Figures 11c and 11d are obtained with $E_b = 2.2\ u_0$.

tests are used in Eqs. 12b–15b and 21b–25b to determine the zone flow rates and switching time of the equilibrium design, which are listed in the parentheses in Table 5. Notice that the experimental flow rates and switching time are slightly different from those calculated for the equilibrium design which does not consider spreading due to mass-transfer effects. The equilibrium design does not give sufficiently high product purities as indicated by the computer simulation results in Table 5. The E_b values estimated from the empirical correlation and the K_f values estimated from batch elution tests are used in the simulations. To overcome the effects of band spreading and get higher product purities, the flow rates in zones I and II have to be decreased and those of zones III and IV have to be increased. Such flow rate changes also result in a lower feed flow rate than the given feed flow rate. In order to keep the same feed flow rate, the average port movement velocity has to be increased (Eq. 25b). The following procedure is used to modify the equilibrium design. A higher feed flow rate than required is used in deriving the flow rates and switching time for a preliminary equilibrium design. The flow rates are then modified to take into account mass-transfer effects. The switching time is shortened to maintain the given feed flow rate. Computer simulations are used to check product concentrations, purities, and yield of the updated design. This procedure is repeated until the product purities are satisfactory. The resulted zone flow rates and switching time are listed in Table 5 outside the parentheses. The equilibrium design gives high product concentrations, and low purities and recoveries in comparison to those from the updated design which takes into account mass-transfer effects (Table 5).

In a previous study for linear isotherm systems with significant mass-transfer effects, modification of the flow rates and switching time of the equilibrium design that is needed to overcome spreading due to mass-transfer effects can be cal-

Table 5. Simulation Parameters and Results for Figure 13

Single Column	R (μm) 162.5	L (cm) 103.2	ϵ_b 0.363	$K_e\epsilon_p$ 0.25	ID (cm) 2.566
SMB system		Zone I	Zone II	Zone III	Zone IV
	$^{**}E_b$ (cm^2/min)	41.821	29.404	41.821	34.909
	K_{f1} (1/min)	1.168	1.168	1.168	1.168
	K_{f2} (1/min)	1.168	1.168	1.168	1.168
	L (cm)	206.4	206.4	206.4	206.4
	F_r (cm^3/min)	35.70 (32.10)	25.10 (24.75)	35.70 (30.40)	29.80 (26.20)
		Raffinate	Extract	Desorbent	Step (min)
Flow rate (mL/min)		10.60 (7.35)	5.90 (4.19)	10.6 (5.65)	10.65 (12.24)
Concentrations		206 (295)	320 (417)		
Purities		93.7% (89.4%)	93.8% (93.6%)		
Recoveries		94.3% (94.0%)	92.9% (85.9%)		
Langmuir Isotherm		a_1^* 0.0948	b_1 −0.00085	a_2^* 0.3073	b_2 −0.00025
Feed Concentrations		C_{f1} (g/L) (Glucose) 398.1		C_{f2} (g/L) (Fructose) 344.6	
Model Approach Fix Bed		Elements 280		Collocs. 3	Δt (min) 0.026

*The adsorbed-phase concentration is based on solid volume. The quoted flow rates and switching time are derived from Eqs. 12b–15b and 21b–25b based on feed concentrations.

$^{**}E_b = 2.2 \times u_0$.

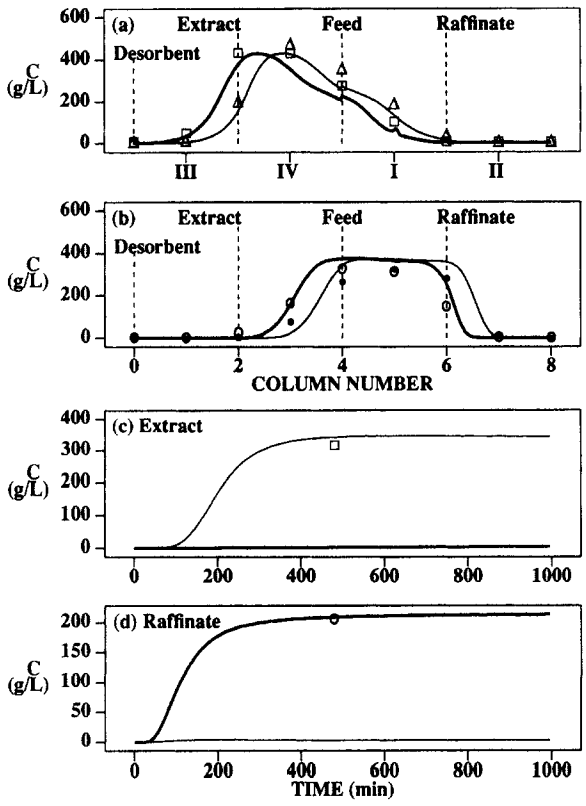

Figure 12. Simulation (lines) vs. experimental data (symbols) for the separation of fructose from glucose using the MiniADSEP SMB system with 1-in.-dia. columns.

Mass-transfer parameters are listed in Table 5. E_b was estimated from the Chund and Wen correlation. (a) Steady-state column profiles for fructose obtained at the midcycle (thick line from simulation, squares from data) and end of a cycle (thin line from simulation, deltas from data); (b) column profiles for glucose, similar convention as in (a) is used; (c) effluent history at the extract port; (d) effluent history at the raffinate port.

culated from column capacity factors, mass-transfer parameters, zone lengths, and desired product purities (Ma and Wang, 1997). The modified design based on the linear theory can serve as an initial guess in the aforementioned iterative procedure in the design of nonlinear systems with mass-transfer effects. The flow rate changes based on linear theory, which satisfy Eqs. 12a and 15a, give more conservative flow rates (that is, higher zone flow rates in zones III and IV and lower flow rates in zones I and II) than those from Eqs. 12b–15b. Therefore, for most systems, the modified flow rates using the linear theory can serve as the upper bounds and those from the equilibrium analysis (Eqs. 12–15 and Eqs. 21–25) as lower bounds in the search for the optimal.

Figures 12a (fructose) and 12b (glucose) compare the experimental column profiles with the simulated column profiles at the middle (bold line) and the end (thin line) of a cycle at $t = 852$ min. In Figure 12a, the squares are obtained at the midcycle time and the deltas are obtained at the end of a cycle. In the simulation, the isotherm parameters are based on the equilibrium tests (Figure 9), and the E_b and K_f are the same as in Figures 10 and 11 (thick lines). The close agreement between experimental data and simulations indicates that the effects of extra-column dispersion in the MiniADSEP are negligible, because the K_f and E_b values obtained using the single column, which has little extra-column dispersion effects, give close predictions of the SMB column profile of fructose. In Figure 12b, the circles are obtained at midcycle and the bullets are obtained at the end of the cycle. The figure shows that the experimental glucose profile, especially the desorption wave in zone IV, is more spread than the simulated profile based on the E_b from the Chung and Wen correlation. This is likely due to viscous fingering as shown in the stepwise elution (washing) tests in Figures 11c and 11d. This hypothesis is confirmed by the simulation results shown in Figure 13.

Figure 13 compares the data with the simulation results obtained with the same parameters as in Figure 12 except that the empirical relation $E_b = 2.2u_0$ is used in order to take into account the viscous fingering effects on the desorption wave of glucose. The agreement between the experimental and simulated column profiles of glucose is improved, but the simulated fructose profile is slightly more spread than the data. This result indicates that the viscous fingering effects on the fructose desorption wave in zone III are less than those on the desorption wave of glucose in zone IV, in which the total sugar concentration is the highest. The predicted product concentrations at steady state agree closely with the data. The experimental concentrations are 314.0 g/L of fructose in

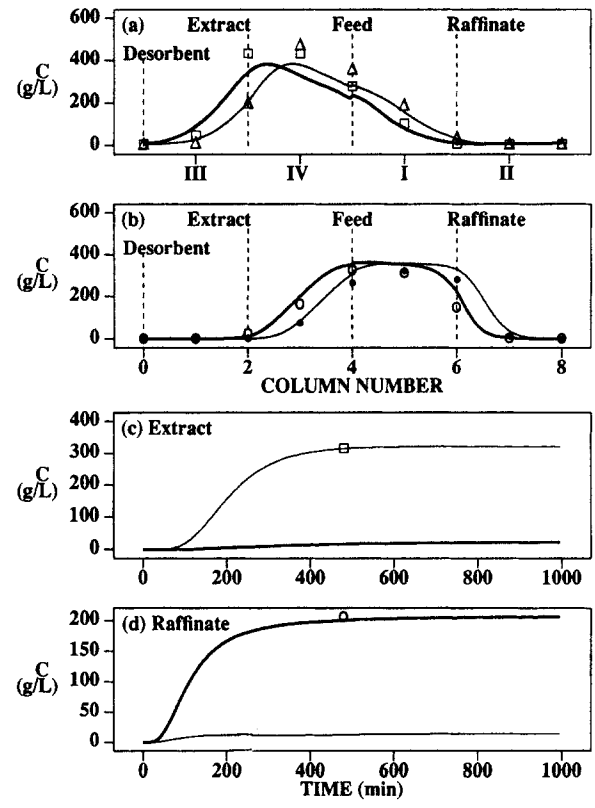

Figure 13. Figure 12 rerun with an empirical correlation $E_b = 2.2\ u_0$.

The simulation parameters are listed in Table 5. Same convention as in Figure 12 is used.

the extract and 205.6 g/L of glucose in the raffinate, while those from simulation are 320.4 in the extract and 205.3 in the raffinate.

Figure 14 compares the experimental profiles with simulations based on the E_b values estimated from the empirical correlation (Table 6) for the ADSEP SMB. Each data point on the experimental profile is the average concentration of a sample collected at the sampling port over an entire cycle. Each experimental profile should lie between the simulated profile at the beginning of a cycle and that at the end of a cycle. Since the concentration at the sampling port is not a linear function of time, the experimental profile is not expected to coincide with the simulated profile at midcycle. The results of Figure 14 show that the data are reasonably close to the simulations. Again for the same reason as explained in Figure 12, the flow rates are different from those calculated from Eqs. 21b–25b in order to counterbalance the mass-transfer effects. The simulated product concentrations are 244.1 (g/L) of glucose in the raffinate and 322.4 (g/L) of fructose in the extract and those from the experiment are 221.3 (g/L) and 324.2 (g/L), respectively. The purities and recoveries are improved and the product concentrations are decreased compared to those obtained with the equilibrium design (in parentheses, Table 5).

The product concentrations and purities at cyclic steady state in Figure 14 are lower than those in Figure 4, which are predicted using the same parameters as in Figure 14 except the E_b values are estimated from the Chung and Wen correlation. The results of Figure 4 suggest that in the absence of viscous fingering effects and extra-column dispersion, ADSEP operated at the flow rates and switching time based on the equilibrium design (without any flow rate modification) can give 99.9% pure extract and raffinate products and their concentrations are higher than those in Figure 14. With viscous fingering and extra-column dispersion effects, ADSEP can still give relatively pure products if the flow

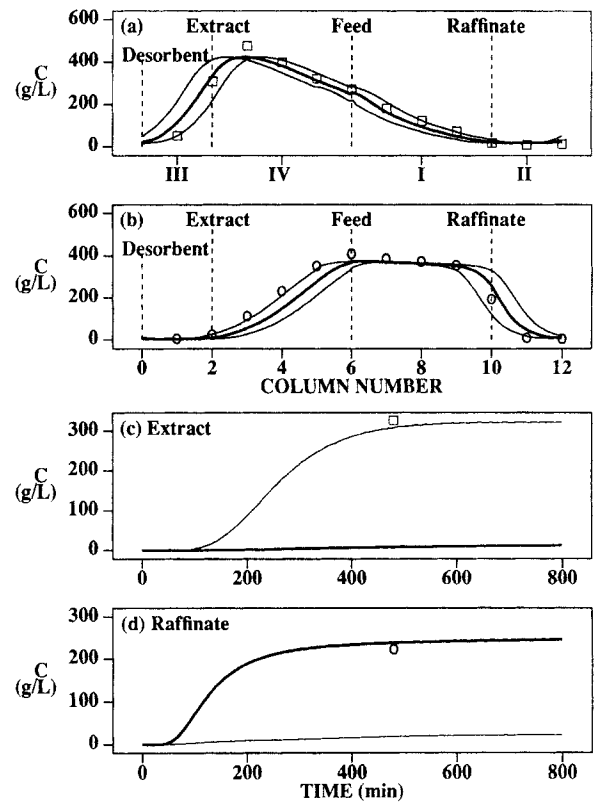

Figure 14. Simulation (lines) vs. experimental data (symbols) for the separation of fructose from glucose using ADSEP SMB with 6-in. columns.

The simulation parameters are listed in Table 6. Same convention as in Figure 12 is used. Thin lines are the simulation profiles at the beginning and end of a cycle. Thick line is the midcycle profile. Squares are the experimental profile for fructose and circles are the experimental profile for glucose.

Table 6. Simulation Parameters and Results for Figure 14

Single Column	R (μm)	L (cm)	ϵ_b^*	$K_c\epsilon_p$	ID (cm)
	162.5	63.5	0.402	0.25	16.15
SMB system		Zone I	Zone II	Zone III	Zone IV
	E_b (cm^2/min)	40.67 (39.03)	30.11 (30.66)	40.10 (36.91)	33.95 (32.31)
	K_{f1} (1/min)	1.168	1.168	1.168	1.168
	K_{f2} (1/min)	1.168	1.168	1.168	1.168
	L (cm)	254	127	127	254
	F_r (mL/min)	1,514 (1,453)	1,121 (1,141)	1,493 (1,374)	1,264 (1,202)
		Raffinate	Extract	Desorbent	Step (min)
Flow rate (mL/min)		393 (312)	229 (172)	372 (233)	6.42 (6.75)
Concentrations		245 (296)	321 (389)		
Purities		91.8% (86.2%)	96.9% (92.3%)		
Recoveries		95.6% (91.4%)	90.7% (82.1%)		
Langmuir Isotherm		a_1^*	b_1	a_2^*	b_2
		0.0948	−0.00085	0.3073	−0.00025
Feed Concentrations		C_{f1} (g/L) (Glucose)		C_{f2} (g/L) (Fructose)	
		403.3		324.2	
Model Approach Fixed Bed		Elements		Collocs.	Δt (min)
		120		3	0.01

*The adsorbed phase concentration is based on solid volume.
$E_b^* = 2.2 \times u_0$.
The quoted flow rates and switching time are derived from Eqs. 12b–15b and 21b–25b.

rates and switching time are modified to take into account the dispersion effects.

The close agreement between experimental data and simulation for the two SMB systems shows that the proposed design approach with standing wave analysis indeed gives robust and optimal designs of nonlinear SMB systems.

Conclusions

General design criteria were derived from the standing wave analysis for nonlinear isotherm systems with negligible mass-transfer resistances. This approach significantly reduced the search effort for the optimal flow rates and switching time. The hodograph analysis was used for the calculation of the interstitial and bed moving velocities for systems without mass-transfer effects. The optimal design was found by iteratively updating the port switching time and the flow rates according to the steady-state concentrations obtained from the equilibrium analysis.

The proposed standing wave design method was tested with numerical simulations for CMB and SMB operations. For systems without significant mass-transfer effects, the column profiles and transient histories of CMB are sharper than those for SMB. However, the product purities at steady state are similar. For systems with significant mass-transfer effects, both the column profiles and effluent histories are almost identical. The results showed that the design approach derived for CMB give robust and optimal flow rates and switching time for SMB systems.

Two pilot-scale SMB systems for the separation of fructose from glucose were studied. Batch tests were used to estimate the isotherm parameters. The anti-Langmuir equation correlated the single component isotherm data closely, but underpredicted the interference in mixtures. Pulse and breakthrough tests were used to estimate mass-transfer parameters for the simulations. Viscous fingering effects were found to increase significantly the spreading of the desorption waves of the low affinity solute. Such effects can be taken into account by the empirical correlation for the axial dispersion coefficient. Viscous fingering and extra-column dispersion effects can be taken into account in the design to produce relatively pure products, but they result in more dilute products compared to a system without these effects. Experimental SMB column profiles and product concentrations were in agreement with simulation results. This study shows that (1) the model used in the simulation gives reasonable predictions of column profiles and product concentrations from the two pilot-scale systems; (2) design and scale-up of SMB can be facilitated with the method introduced in this study.

Acknowledgments

This research has been supported by grants from NSF (GER9024174), the Peterson Foundation, and the Showalter Foundation.

Notation

A = constant
E_b = axial dispersion coefficient
F = volumetric flow rate
L = zone length
L_c = column length
S = column cross-section area
a = Langmuir isotherm constant
b = Langmuir isotherm constant
c = liquid-phase concentration
c_b = bulk phase concentration
c^* = averaged pore phase concentration (over particle volume)
d_p = particle diameter
q = solid phase concentration
t_0 = dead time
t_s = port switching time
v = solid movement linear velocity ($v = L_c/t_s$)
x = position inside the bed

Subscripts

b = bulk phase
i = index
s = steady-state or concentration dependent
f = feed concentration or film mass transfer
w = net linear velocity

Literature Cited

Adachi, S., "Simulated Moving-Bed Chromatography for Continuous Separation of Two Components and Its Application to Bioreactors," *J. Chromatog. A*, **658**, 271 (1994).

Broughton, D. B., "Molex: Case History of a Process," *Chem. Eng. Prog.*, **64**, 60 (1968).

Broughton, D. B., R. W. Neuzil, J. M. Pharis, and C. S. Brearley, "The Parex Process for Recovering Paraxylene," *Chem. Eng. Prog.*, **66**, 70 (1970).

Ching, C. B., C. Ho, and D. M. Ruthven, "Experimental Study of a Simulated Countercurrent Adsorption System—VI. Non-linear Systems," *Chem. Eng. Sci.*, **43**(3), 703 (1988).

Ching, C. B., K. H. Chu, K. Hidajat, and M. S. Uddin, "Experimental and Modeling Studies on the Transient Behavior of a Simulated Countercurrent Adsorber," *J. of Chem. Eng. Japan*, **24**(5), 614 (1991).

Ching, C. B., K. H. Chu, K. Hidajat, and M. S. Uddin, "Comparative Study of Flow Schemes for a Simulated Countercurrent Adsorption Separation Process," *AIChE J.*, **38**, 1744 (1992).

Ching, C. B., K. H. Chu, K. Hidajat, and D. M. Ruthven, "Experimental Study of a Simulated Counter-current Adsorption System: VII. Effects of Non-linear and Interacting Isotherms," *Chem. Eng. Sci.*, **48**, 1343 (1993).

Chung, S. F., and C. Y. Wen, "Longitudinal Dispersion of Liquid Flowing Through Fixed and Fluidized Beds," *AIChE J.*, **14**, 857 (1968).

Corbett., J., and D. Burke, "System Optimization in the Chromatographic Separation of Fructose from Dextrose in the Corn Wet Milling Industry," Symp. on Industrial Scale Process Chromatog. Sep., New Orleans (Mar. 1996).

Ernest, M. V., Jr., J. P. Bibler, R. D. Whitley, and N.-H. L. Wang, "Development of a Carousel Ion-Exchange Process for Removal of Cesium-137 from Alkaline Nuclear Waste," *Ind. Eng. Chem. Res.*, **36**, 2775 (1997).

Ganetsos, G., and P. E. Barker, eds., *Preparative and Production Scale Chromatography*, Marcel Dekker, New York (1993).

Glueckauf, E., "Ion-Exchange and Its Applications," Soc. of Chem. Ind., London, p. 34 (1955).

Katti, A., Z. Ma, and G. Guiochon, "Prediction of Binary, Overloaded Profiles Using the Simple Wave Effect," *AIChE J.*, **36**, 1722 (1990).

Ma, Z., and G. Guiochon, "Whole Column Simulation in Nonlinear Chromatography: Traveling Characteristics of the Concentration Waves of a Binary Mixture," *Anal. Chem.*, **62**, 2330 (1990a).

Ma, Z., A. Katti, B. Lin, and G. Guiochon, "Simple Wave Effects in Two-Component Nonlinear Liquid Chromatography. Application to the Measurement of Competitive Adsorption Isotherms," *J. Phys. Chem.*, **94**, 6911 (1990b).

Ma, Z., and G. Guiochon, "Application of Orthogonal Collocation on Finite Elements in the Simulation of Non-linear Chromatography," *Comput. Chem. Eng.*, **15**, 415 (1991).

Ma, Z., R. D. Whitley, and N.-H. L. Wang, "Pore and Surface Diffu-

sion in Multicomponent Adsorption and Liquid Chromatography Systems," *AIChE J.*, **42**, 1244 (1996).
Ma, Z., and N.-H. L. Wang, "Design of Simulated Moving Bed Chromatography Using Standing Wave Analysis: Linear Systems," *AIChE J.*, **43**, 2488 (1997).
Mackie, J. S., and P. Meares, "The Diffusion of Electrolytes in a Cation-Exchange Resin Membrane," *Proc. Roy. Soc. London Ser. A.*, **232**, 498 (1955).
Mazzotti, M., G. Storti, and M. Morbidelli, "Robust Design of Countercurrent Adsorption Separation Processes: 2. Multicomponent Systems," *AIChE J.*, **40**, 1825 (1994).
Mazzotti, M., G. Storti, and M. Morbidelli, "Robust Design of Countercurrent Adsorption Separation Processes: 3. Nonstoichiometric Systems," *AIChE J.*, **42**(11), 2784 (1996).
Rhee, H.-K., R. Aris, and N. R. Amundson, "On the Theory of Multicomponent Chromatography," *Phil. Trans. Roy. Soc. London A.*, **267**, 419 (1970).
Rhee, H.-K., R. Aris, and N. R. Amundson, "Multicomponent Adsorption in Continuous Countercurrent Exchangers," *Phil. Trans. Roy. Soc. London A.*, **269**, 187 (1971).
Rhee, H.-K., R. Aris, and N. R. Amundson, *First-Order Partial Differential Equations*, Vol. 2, Prentice Hall, Englewood Cliffs, NJ (1989).
Ruthven, D., and C. B. Ching, "Counter-Current and Simulated Counter-Current Adsorption Separation Processes," *Chem. Eng. Sci.*, **44**, 1011 (1989).
Santacesaria, E., M. Morbidelli, A. Servida, G. Storti, and S. Carra, "Separation of Xylenes on Y Zeolites. 2. Breakthrough Curves and Their Interpretation," *Ind. Eng. Chem. Process Des. Dev.*, **21**, 446 (1982).
Storti, G., M. Masi, S. Carra, and M. Morbidelli, "Optimal Design of Multicomponent Countercurrent Adsorption Separation Processes Involving Nonlinear Equilibria," *Chem. Eng. Sci.*, **44**, 1329 (1989).
Storti, G., M. Mazzotti, M. Morbidelli, and S. Carra, "Robust Design of Binary Countercurrent Adsorption Separation Processes," *AIChE J.*, **39**, 471 (1993).
Storti, G., R. Baciocchi, M. Mazzotti, and M. Morbidelli, "Design of Optimal Operating Conditions of Simulated Moving Bed Adsorptive Separation Units," *Ind. Eng. Chem. Res.*, **34**, 288 (1995).
Ulrich, P. E., and J. T. Hsu, "Study of Simulated Moving-Bed Separation Processes Using a Staged Model," *Ind. Eng. Chem. Res.*, **28**, 1211 (1989).
Wilson, E. J., and C. J. Geankoplis, "Liquid Mass Transfer at Very Low Reynolds Numbers in Packed Beds," *Ind. Eng. Chem. Fundam.*, **5**, 9 (1966).
Wu, D.-J., Z. Ma, B. W. Au, and N.-H. L. Wang, "Recovery and Purification of Paclitaxel Using Low-Pressure Chromatography," *AIChE J.*, **43**, 232 (1997).

Manuscript received June 5, 1997, and revision received Sept. 30, 1998.